



HAL
open science

Development and validation of a thermally regulated atmospheric simulation chamber (THALAMOS): A versatile tool to simulate atmospheric processes

Noureddin Osseiran, Manolis Romanias, Vincent Gaudion, Maria Angelaki, Vassileios Papadimitriou, Alexandre Tomas, Patrice Coddeville, Frederic Thevenet

► To cite this version:

Noureddin Osseiran, Manolis Romanias, Vincent Gaudion, Maria Angelaki, Vassileios Papadimitriou, et al.. Development and validation of a thermally regulated atmospheric simulation chamber (THALAMOS): A versatile tool to simulate atmospheric processes. *Journal of Environmental Sciences*, 2020, 95, pp.141-154. 10.1016/j.jes.2020.03.036 . hal-02913609

HAL Id: hal-02913609

<https://hal.science/hal-02913609>

Submitted on 18 Jul 2022

HAL is a multi-disciplinary open access archive for the deposit and dissemination of scientific research documents, whether they are published or not. The documents may come from teaching and research institutions in France or abroad, or from public or private research centers.

L'archive ouverte pluridisciplinaire **HAL**, est destinée au dépôt et à la diffusion de documents scientifiques de niveau recherche, publiés ou non, émanant des établissements d'enseignement et de recherche français ou étrangers, des laboratoires publics ou privés.



Distributed under a Creative Commons Attribution - NonCommercial 4.0 International License

1 **Development and validation of a thermally regulated atmospheric simulation chamber**
2 **(THALAMOS): A versatile tool to simulate atmospheric processes**

3
4 Nouredin Osseiran¹, Manolis N. Romanias^{1,*}, Vincent Gaudion¹, Maria E. Angelaki²,
5 Vassileios C. Papadimitriou^{2,*}, Alexandre Tomas¹, Patrice Coddeville¹, Frederic Thevenet¹

6
7 1. IMT Lille Douai, Univ. Lille, SAGE, Lille F-59000, France

8 2. Laboratory of photochemistry and chemical kinetics (LAPKIN), University of Crete,
9 Heraklion 71003, Crete, Greece

10

11

Abstract

12
13 Atmospheric simulation chambers, are unique tools for investigating atmospheric processes in the gas
14 and heterogeneous phases. They can provide a controlled yet realistic environment that simulates
15 atmospheric conditions. In the current study, a Teflon atmospheric simulation chamber of 600 L,
16 named THALAMOS (thermally regulated atmospheric simulation chamber) has been developed and
17 cross-validated. THALAMOS can be operated over the temperature range 233 to 373 K under both
18 static and flow conditions. It is equipped with state of the art instrumentation (selective ion flow tube
19 mass spectrometry (SIFT-MS), long path Fourier transform infrared spectroscopy (FTIR), gas
20 chromatography mass spectrometry (GC-MS), various analyzers) for the inline monitoring of both
21 reactants and products. THALAMOS was validated by measuring the rate coefficients of well
22 documented reactions, i.e. the reaction of ethanol with OH radicals and the reaction of
23 dichloromethane with Cl atoms, in a wide temperature range. Two different detection techniques were
24 used in parallel, FTIR and SIFT-MS, to internally cross-validate the obtained results. The measured
25 rate coefficients are in excellent agreement both between each other and with the literature
26 recommended values. Furthermore, the gas phase oxidation of toluene by Cl atoms (kinetics and
27 product yields) was studied in the temperature range of 253 to 333 K. To the best of our knowledge,
28 THALAMOS is a unique facility on national level and among a few smog chambers internationally
29 that can be operated in such a wide temperature range providing the scientific community with a
30 versatile tool to simulate both outdoor and indoor physicochemical processes.

31 **Keywords:**

32 Thermostated simulation chamber

33 Gas phase kinetics

34 Cl initiated degradation of toluene

35 Benzaldehyde

36 -----

37 * Corresponding authors. E-mails: emmanouil.romanias@imt-lille-douai.fr (Manolis N.
38 Romanias), bpadim@uoc.gr (Vassileios C. Papadimitriou)

39

Introduction

40
41
42 Air pollution is one of the major concerns of our society nowadays. The intense anthropogenic
43 activities related to combustion, industrialization, agriculture and livestock, release a wide variety of
44 pollutants in the atmosphere affecting air quality. Furthermore, in the context of climate change and
45 the anticipated global temperature change, as well as the increasing urbanization rate observed within
46 the last 70 years (in 2015 around 80% of the population was living in urban areas in developed
47 countries (United Nations, 2018)), the effects on air quality have been a top priority issue in the
48 agenda of many countries. Therefore, a strong effort has been made by the atmospheric science
49 community through multidisciplinary actions involving laboratory, field and modeling studies aiming
50 to elucidate the important processes that lead to air pollution, to propose solutions and to make
51 predictions regarding the future Earth's climate.

52 Hence, the thorough study of chemical processes occurring during night time or daytime in the
53 atmosphere, is of great importance in order to (i) elucidate the fate of pollutants and investigate their
54 impact to the physicochemical properties of the atmosphere, e.g., formation of organic aerosols and
55 tropospheric O₃, stratospheric ozone depletion as well as to (ii) determine the lifetimes of pollutants
56 and thus their impact on the future climate. However, the atmosphere is an open chemical reactor and
57 thus the direct control or isolation of chemical processes is challenging. Alternatively, in laboratory
58 scale the investigation of key atmospheric phenomena can occur inside Atmospheric Simulation
59 Chambers (ASC). ASC provide a controlled, yet realistic environment, aiming to simulating
60 atmospheric conditions without any meteorological or emissive influences that occur in real
61 atmosphere. Since the first ASC development (Akimoto et al., 1979; Leone et al., 1985) in the mid-
62 1980s, several small to large-scale facilities have been developed worldwide aiming to study (i) gas
63 phase reactions between the major atmospheric oxidants and both anthropogenic and biogenic volatile
64 organic compounds (VOCs), (ii) secondary organic aerosol (SOA) formation and (iii) nucleation
65 phenomena, and/or processes related with air-quality and climate. In Europe, most of these facilities
66 are integrated in the Eurochamp-2020 project and are accessible to the scientific community (Huang et
67 al., 2012).

68 Generally, there are two types of simulation chambers: indoor and outdoor. They are also present in a
69 wide range of volumes and forms, and can be constructed by several materials including Teflon, Pyrex
70 glass, stainless steel etc. However, till today, the majority of simulation chambers studies, especially
71 the ones related to gas-phase chemistry, have been conducted close to ambient temperature and sea
72 level pressure conditions. Atmospheric pressure and temperature though vary with the altitude.
73 Particularly, temperature variation can strongly affect physicochemical phenomena (i.e. kinetics,
74 reaction mechanism, nucleation processes, etc.) and plays a key role in several atmospheric studies.

75 Therefore, the objective of this study was to develop and validate an atmospheric simulation chamber,
76 named THALAMOS (thermally regulated atmospheric simulation chamber), that can be used as a
77 reference tool for temperature dependent studies simulating both outdoor and indoor environment. In
78 this paper, we introduce THALAMOS to the scientific community presenting a detailed description of
79 chambers' characteristics and capabilities. To the best of our knowledge, THALAMOS is the first
80 ASC, in national level that allows temperature dependent studies, and one of very few facilities
81 globally, with such a wide accessible temperature range, 233 – 373 K that fully covers relevant to the
82 troposphere temperature range and can also be operated at higher temperatures either to study extreme
83 indoor conditions or to investigate reaction mechanism. Within this framework, a series of results that
84 demonstrate both THALAMOS validity as a versatile tool for temperature dependent kinetics and end-
85 products determination as well as the extent of its capabilities are presented herein. First,
86 THALAMOS was validated by measuring the kinetics of the well documented gas phase reactions of
87 OH radicals and Cl atoms with ethanol and dichloromethane (DCM), over a wide temperature range.
88 Next, the Cl atoms rate coefficients for the gas phase reaction of Cl atoms with toluene were measured
89 and the reaction mechanism was investigated, as a function of temperature. Finally, the obtained
90 results are discussed. Toluene is an aromatic compound mainly emitted by anthropogenic activities
91 and concentrations that can reach up to several hundreds of ppbV in outdoor (Hazrati et al., 2016) or
92 working indoor environments (Can et al., 2015).

93 1. Materials and methods

94 1.1 THALAMOS description and characteristics

95 THALAMOS is an indoor, atmospheric simulation chamber with a volume of 0.6 m³ (**Fig. 1**) that
96 consists of three main parts, (i) a climatic thermostatic cage (VT-4100, Vötsch industrietechnik,
97 Germany), (ii) a Teflon chamber of cuboid shape attached on an aluminum frame (see **Fig. 1**) and (iii)
98 multiple inline complementary detection techniques, such as Fourier transform infrared spectroscopy
99 (FTIR), selective ion flow tube mass spectrometry (SIFT-MS), and gas chromatography mass
100 spectrometry (GC-MS) that they are assembled externally to the Teflon-chamber. The thermostatic
101 cage (or climatic box) has an effective volume of 1200 L and the temperature can be regulated
102 between 231 and 453 K. The climatic box is equipped with a platinum temperature sensor (PT-100,
103 Pico technology, France) to measure the temperature and two fans to transfer and homogenize the
104 heated/cooled air in the thermostatic cage (**Fig. 1**). **Fig. 2** displays the temperature change rate inside
105 the climatic box illustrating the facility efficiency to achieve extreme cold or hot conditions in a
106 relatively short time window and to adequately simulate the relevant to the Troposphere conditions, in
107 a very well-controlled environment inside the Teflon-chamber.

108 The Teflon chamber volume was experimentally determined via absolute concentration measurement
109 of ethylbenzene by employing Beer-Lambert law and using in-line infrared spectroscopy. Particularly,
110 multiple titrated volumes of liquid ethyl-benzene (C₆H₅CH₂CH₃) were introduced via micro-syringe
111 into the chamber, i.e., 0.1 – 0.5 mL, and the infrared (IR) spectra were recorded using 1 cm⁻¹
112 resolution and 128 co-added scans. IR spectra were integrated between 2493 and 3492 cm⁻¹. Using an
113 integrated band strength of 3.36×10^{-17} cm²/(molecule·cm), and a density of 0.8626 g/cm³ for ethyl-
114 benzene, chamber volume was determined to be 601 ± 6 L (Lide, 2005). A temperature and pressure
115 sensor were assorted in the center and back side of the Teflon chamber (see **Fig. 1**) and the gas
116 mixture temperature/pressure were monitored in real-time. Both measurements were digitized and
117 recorded and stored in a lab computer for further analysis.

118 The Teflon chamber is also equipped with four fans to ensure (i) the temperature homogeneity of the
119 gas mixture and (ii) the efficient mixing of reagents. Particularly, the two fans are placed at the front

120 and bottom-right side of the chamber, right after the inlet port and installed with a 45 degrees angle
121 allowing the efficient transport of the injected compounds to the main body of the chamber. Two more
122 fans are placed at the back and up-left side (**Fig. 1**). The temperature inside the thermostatic cage and
123 the Teflon chamber were measured via two thermocouples and the readings comparison over a wide
124 range are comparatively depicted in Appendix A **Fig. S1**. An excellent agreement - differences are
125 lower than 1% in Kelvin scale, validating that the gas mixture in the Teflon chamber is effectively
126 thermally-equilibrated throughout the reactor volume.

127 1.1.1 Admission and mixing of compounds

128 A multi-inlet port placed in the front and bottom-right side of the chamber was used for compounds
129 introduction (**Fig. 1**). Depending on the physical state and volatility of compounds, different injection
130 methods were applied.

131 (i) Injection of gas phase compounds

132 Gases are introduced in the chamber either using gas syringes or via controlled flow through mass
133 flow controllers.

134 (ii) Injection of liquid phase compounds

135 For the injection of liquid phase compounds two different methods were applied. In the first method,
136 liquid compounds were injected inside the chamber via a septum inlet using syringes, under a stream
137 of zero-air. To facilitate the evaporation of the liquid, the introduction line was heated at 323 K by
138 using heating taped inlets to control the temperature. Nevertheless, to ensure complete vaporization of
139 the injected compounds, inlet-line's temperature can be increased up to 423 K, when needed, in the
140 case of very low-volatile compounds. In the second method, gas mixtures of known concentrations
141 were prepared in zero air and injected using mass flow controllers. In particular, compounds in the
142 liquid phase were transferred to a glass tube that could be thermostated. Then using gas handling
143 system equipped with Baratron pressure gauges compounds' were either collected in 10 L glass bulb
144 or to a 6 L Silonite canister (both were previously evacuated to a pressure of 10^{-3} mbar) and further
145 diluted to a total pressure of 1300 mbar for the glass bulb and 2070 mbar for Silonite canister using

146 zero air as bath gas. The manometrically prepared mixtures were injected in the chamber using mass
147 flow controllers under zero air stream.

148 (iii) Mixing of compounds

149 Gas mixture homogenization inside THALAMOS, at 296 K, is achieved within ~1 min, but in general,
150 it is also dependent on compound volatility, potent adsorption, hydrolysis or condensation onto
151 chamber's surface and THALAMOS temperature. To ensure steady-state concentrations for all the
152 species in the chamber, gas mixture was fan-mixed for, at least, 20 min before reaction's initiation,
153 and the gas phase concentrations of the organic compounds were continuously monitored to warrant
154 steady-state using the analytical instrumentation described below.

155 1.1.2 Bath gas and Teflon chamber cleaning

156 In the majority of the THALAMOS runs, zero air is being used as bath gas, generated from an oil-free
157 air-compressor, coupled with an inline water removal system. Then, zero air could be further purified
158 and is provided to the chamber under a regulated constant flow. Depending on the purification
159 process, two different zero air flows can be used. In the first case, the air produced is driven through a
160 zero air generator (AZ-2020, Claind, Italy) operated at 673 K to catalytically convert the organics
161 present in the air flow to CO₂. The exact relative humidity (RH) in the gas flow at room temperature,
162 293 K, was determined to be 2% using a temperature and relative humidity probe (HQ 210, Kimo,
163 France) with an accuracy $\pm 1\%$ as stated by the manufacturer. Alternatively, the air flow from the
164 compressor is sent to a high purification system (zero-air generator equipped with a pressure swing
165 adsorption (PSA) device), where volatile organic compounds (VOCs), CO₂, CO and H₂O are removed.
166 The remaining impurity levels in the air stream are always lower than the analytical system detection
167 limits: VOCs < 0.1 ppbV, CO₂ < 10 ppbV, CO < 80 ppbV and H₂O ~ 2 ppmV at 293 K. We estimate
168 that NO_x and O₃ concentration levels in the chamber are below 50 and 500 pptV respectively
169 (detection limits of NO_x analyzer (T200 UP, Teledyne, USA) and ozone analyzer (APOA 370, Horiba,
170 France)). In addition, it is important to mention that when measurements in the presence of NO_x are
171 carried out in THALAMOS, right after their completion the Teflon film of the chamber, the tubing's

172 and even the diaphragm in the Teflon pump are replaced to ensure that our system is clean and free of
173 any memory effects in the future experiments.

174 Prior to each experiment, THALAMOS is flushed-out for at least 2 hours, using a constant flow of
175 zero-air, i.e., 20 L/min and a similar pumped-out rate. The cleaning process is necessary in order to
176 avoid any side reaction or accumulation of different reactants inside the chamber or dead-volumes,
177 eliminating memory effects during sequential experiments.

178 1.1.3 Light sources and radicals/atoms precursors and production

179 In order to induce photo-oxidation reactions, the thermostatic cage has been equipped with a light
180 irradiation system capable to host 20 lamps. More specifically, the attached broad-band emission light
181 sources are (i) 10 ultraviolet (UV) lamps emitting in the A region of electromagnetic spectrum, i.e.
182 UV-A lamps (PL-L 24W/10/4P, Philips, Netherlands) with a maximum wavelength (λ_{\max}) at 365 nm,
183 and (ii) 10 mercury lamps (HNS-L 24W 2G11, Osram, UK) emitting UV radiation in the C region of
184 the electromagnetic spectrum, i.e. UV-C lamps, with a λ_{\max} at 254 nm. Therefore, THALAMOS can
185 be used to study any induced processes in the gas phase (e.g. photolysis of compounds of interest, or
186 cross section measurements) or involving heterogeneous phase (e.g., TiO₂ photocatalysis). It should be
187 noted that the heat released from the lamps (when switched on) does not impact the temperature inside
188 THALAMOS. In particular, the response of the climatic box to temperature variations has been settled
189 to a minimum of ± 1 K, which is feasible due to the high performance of our heating/cooling system.
190 Gas mixture temperature inside THALAMOS is maintained stable (± 1 K) and any variations are
191 continuously monitored, both inside and outside the Teflon chamber, during the course of all the
192 photochemical experiments.

193 In the current study, UV-A lamps were used to generate Cl atoms via Cl₂ photolysis:



195 Similarly, the UV-C lamps were used to photolyze H₂O₂ and produce OH radicals via the reaction:



197 where $h\nu$ corresponds to the light source photon-energy.

198 1.1.4 Reaction mixture sampling and detection techniques

199 A Restek Sulfinert-treated stainless steel tube was placed in the center and back-side of the chamber,
200 allowing the reaction mixture sampling off the chamber. Stable reactants and products were
201 continuously monitored via coupling the chamber in series with several detection methods and
202 sensors, with the main ones to be (i) a SIFT-MS (Voice 200 ultra, Syft Technologies, New Zealand),
203 (ii) a multipath FTIR (Antaris IGS, Thermo Scientific, France) with an optical path of 10 m and (iii) a
204 thermal desorption GC-MS (7890A, Agilent Technologies, France). The complementary detection
205 techniques provides with the advantage to identify a great variety of chemical species with high
206 sensitivity and via cross-validation allow to minimize intrinsic uncertainties in temporal loss and
207 formation profiles measurements for reactants and products, respectively. Sample-out rate was
208 adjusted in a case by case experiment, according to the analytical methods employed at each
209 measurement. Particularly, a recycling Teflon diaphragm pump, 4 L/min, is used to create a closed-
210 loop between the chamber and the analytical instruments. In the case that solely SIFT-MS is used,
211 reaction mixture was continuously sampled-out with a flow rate of 5 to 25 mL/min. Given that
212 experiments duration was less than two hours, a negligible gas-mixture volume was lost <0.5%, taking
213 into account experimental uncertainties. FTIR optical cell is part of the closed-loop and thus does not
214 alter the gas volume. Finally, although it was not used in the present study, it is worth to note that GC-
215 MS could be also used simultaneously in THALAMOS, since the amount of the required reaction
216 mixture for the analysis is insignificant (~200 mL/min), compared to THALAMOS volume. It is also
217 worth mentioning that in all cases results were cross-validated using simultaneously at least two
218 independent detection methods, and the required sampling did not result in any measurable alteration
219 of reactants concentrations, within the precision of the measurements.

220 The SIFT-MS is a tandem chemical ionization mass spectrometer based on the chemical ionization of
221 the analytes. A microwave discharge is used for the simultaneous generation of three precursor ions,
222 H_3O^+ , NO^+ and O_2^+ , which are sequentially selected by a first quadrupole mass filter (Smith and
223 Spanel, 2005; Spanel and Smith, 2013). Then, the precursor ions are injected inside a flow tube reactor
224 operated at mTorr pressure using N_2 , as carrier gas. At the same time, the sample is injected at the
225 upstream-end of the reactor. The precursor ions react with the analytes along the flow tube to produce

226 new characteristic ionized molecules (Smith and Spanel, 2005; Spanel and Smith, 2013). It is worth
227 mentioning that both the sampling port and the flow tube of the instrument are heated to 393 K to
228 eliminate contaminations of the sampling line and wall reactions along the flow tube. Subsequently,
229 the gas flow passes through a pinhole orifice of 0.3 mm diameter, located at the downstream end of the
230 flow tube reactor to create a molecular beam. The molecular beam enters a differentially-pumped high
231 vacuum chamber and both the precursor and reaction product-ions are focused, via electrostatic lenses,
232 into a second quadrupole mass spectrometer for mass analysis and ion counting for identification and
233 quantification, respectively. The mass spectrometer is internally calibrated on a daily basis, by flowing
234 a standard mixture of 9 compounds provided by the supplier. The internal calibration procedure and
235 the known reaction rate coefficients of the precursor ions with the analytes, allow estimating the
236 theoretical concentrations of any organic compound. Nevertheless, to obtain accurate concentration
237 measurements, the instrument was regularly calibrated by passing standards of the compounds of
238 interest. Although in kinetic measurements the absolute concentrations are not used, it is worth
239 mentioning that the difference between estimated theoretical concentrations and the ones determined
240 experimentally were in fairly reasonable agreement with the observed differences never being higher
241 than 30%. Instrument's time resolution depends on the number of mass spectral peaks monitored, as
242 well as on the number of the averaging counts. For instance, the real time monitoring of 20 mass
243 spectral intensities with a limit of 10000 counts for each mass, time resolution was ca. 10 sec. Under
244 these conditions the detection limits for ethanol, dichloromethane and toluene were 1, 0.8, and 0.9
245 ppbV, respectively.

246 Complementary to the SIFT-MS, the reaction mixture was simultaneously analyzed employing an
247 FTIR spectrometer equipped with a 10 m path length White-cell, with anti-reflected coated zinc
248 selenide transmission windows. A liquid-N₂ cooled mercury cadmium telluride (MCT) detector was
249 attached and 64 co-added IR spectra were recorded between 650 and 4000 cm⁻¹, with 1 cm⁻¹
250 resolution, using Result-3 software. Quantification and data processing was performed using a thermos
251 scientific software, TQ-AnalystTM, and internally developed routines for kinetic analysis. The optical
252 path was also experimentally calibrated using compounds with well-known IR cross-sections and it

253 was determined to be 10 ± 0.1 m, that is in excellent agreement with manufacturer technical data. The
254 detection limits for ethanol, dichloromethane and toluene were in the ppmV range (~ 1 ppmV).

255 Background IR spectra were collected before compounds injection in the chamber. Note that a Teflon
256 circulating pump was used in a closed loop to ensure gas phase mixture homogeneity between
257 chamber and FT-IR cell. After recording the background, reaction mixture was introduced in the
258 chamber left until it was well-mixed. Well-mixing was verified by recording sequential IR spectra.
259 The stabilization of the concentrations in the Teflon chamber was achieved after a few minutes and
260 was verified by observing stable. The reactants characteristic IR absorption bands reached a steady
261 absorbance (± 1 %) within a few minutes and that was also cross-checked by monitoring the
262 compounds concentration profiles using the SIFT-MS.

263 1.1.5 THALAMOS first-order losses

264 *n*-Pentane (C_5H_{12}) was used as probe molecule aiming to evaluate possible leaks of THALAMOS. In
265 this series of experiments, 30 ppmV of *n*-pentane was injected in the chamber and its temporal profile
266 was monitored for several hours using the SIFT-MS. A typical plot, 293 K, is shown in Appendix A
267 **Fig. S2**. The first order loss of pentane was measured to be $\sim 10^{-6} \text{ sec}^{-1}$ and it is not expected to affect
268 the kinetic measurements. Similar tests were carried-out between 253 and 353 K leading to identical
269 results. However, since wall-loss and on surface hydrolysis is also an intrinsic variable of the
270 compound used (volatility, functionality, chemical affinity, etc.), dark-loss tests were carried-out in a
271 case-by-case basis, before every experimental series runs.

272 1.2 Relative rate measurements

273 In this section THALAMOS validation approach is presented. Two well-studied gas phase reactions,
274 i.e., OH radicals with ethanol (C_2H_5OH) and Cl atoms with dichloromethane (DCM, CH_2Cl_2), were
275 studied between 253 and 363 K at 760 Torr, in the presence of zero air. Further, kinetics and end-
276 oxidation products for the reaction of Cl atoms with toluene (C_7H_8) were also determined. In all cases,
277 the kinetic measurements were performed applying the relative rate method (RR).

278 In RR method the temporal loss of the under study compound (M) is measured relative to that of a
279 reference compound (REF) ensuring that the observed changes are solely due to their reaction with the

280 oxidant of interest X (X: OH, Cl, NO₃, O₃). RR method is a widely used method (Atkinson et al.,
281 2006; Burkholder et al., 2015) and the relative rate coefficient is derived by the expression (King,
282 2016):

$$283 \ln\left(\frac{[M]_0}{[M]_t}\right) = \frac{k_M}{k_{REF}} \ln\left(\frac{[REF]_0}{[REF]_t}\right) \quad (3)$$

284 where [M]₀, [REF]₀, [M]_t, and [REF]_t are the initial concentrations of the compound of interest and
285 that of the reference, at reaction time *t* = 0, and at discrete times (*t*) after reaction mixture irradiation
286 and *k_M* and *k_{REF}* are the corresponding second order rate coefficients, respectively. A relative rate plot,
287 ln([M]₀/[M]_t) versus ln([REF]₀/[REF]_t), should be linear, with a slope equal to rate coefficients ratio,
288 *k_M*/*k_{REF}*, and a zero intercept. Therefore, the rate coefficient for the reaction of interest can be
289 determined from the relative rate data fitting relative to the known rate coefficient of the reference
290 reaction (*k_{REF}*) (King, 2016).

291 Dark loss and photolysis tests were always conducted before rate coefficient measurements to ensure
292 that both reactants are only lost via the reaction with the reactive species, while reactants well-mixing
293 was verified before irradiation. In all measurements presented herein, UV-A and UV-C lamps
294 photolysis loss was negligible for all the compounds the study involves, within the time frame of the
295 experiment, while no measurable dark loss were observed.

296

297 1.3 Experimental protocol

298 Prior to each relative rate experiment, the chamber was continuously flushed with zero air (cleaning
299 process). Next, the background concentrations of the compounds of interest were measured using all
300 the employed detection techniques. In kinetics determinations and at temperatures above 293 K,
301 reactants and radical precursors were introduced in the chamber once the desired chamber temperature
302 had been reached. At lower temperatures than 293 K the reaction mixture was introduced at room
303 temperature and then the desired temperature was set. Reactants concentration was monitored through
304 the whole time until the final temperature adjustment of the chamber to ensure that no wall loss
305 processes were occurred. Two criteria need to be fulfilled before initiating the reaction: (i) the
306 temperature in the climatic box to be equal to ±1 K with that of the gas mixture recorded inside the
307 Teflon chamber, and (ii) the concentration profiles of organic compounds to be stable. Then, the

308 reaction is initiated by switching on the UV-A or UV-C lamps, which photolyzes the OH radicals or
309 Cl atoms precursors, respectively. Reactants consumption and products formation is then continuously
310 recorded, as a function of time.

311 1.4 Materials

312 All chemicals used in the current study are commercially available and listed in Appendix A **Table S1**
313 along with their stated purities. The mass spectrometric ion peaks selected to monitor the
314 concentration profiles of reference and target molecules are listed in **Table 1**.

315

316 2. Results and discussion

317 2.1 THALAMOS validation for kinetic measurements

318 In this section, OH radicals and Cl atoms kinetics for their reaction with ethanol and DCM,
319 respectively, are presented. There were multiple reasons for choosing the abovementioned reactions.
320 First, both reactions are of atmospheric interest; in particular, the study of atmospheric relevant
321 reactions initiated by OH radicals (the major tropospheric oxidant) and Cl atoms (important
322 tropospheric oxidant in coastal and urban areas) is of significant importance in order to determine the
323 fate of pollutants in the atmosphere and thus their impact on air quality and climate change. Secondly,
324 the rate coefficients of both reactions have been extensively studied and the kinetic data have been
325 evaluated by both International Union of Pure and Applied Chemistry (IUPAC) and the National
326 Aeronautics and Space Administration/Jet Propulsion Laboratory (NASA/JPL) Panels. Therefore,
327 these reactions were selected to evaluate THALAMOS reliability to measure relative rate coefficients
328 over a wide temperature range, 253 – 353 K and thus its capability to provide accurate kinetic data of
329 atmospheric relevant reactions.

330 2.1.1 OH radical reaction rate coefficients with ethanol

331 The gas phase reaction of OH radicals with ethanol has been the subject of interest for more than 3
332 decades (Campbell et al., 1976; Dillon et al., 2005; Greenhill and Ogrady, 1986; Jiménez et al., 2003;
333 Kovács et al., 2005; Nelson et al., 1990; Oh and Andino, 2001; Orkin et al., 2011; Overend and
334 Paraskevopoulos, 1978; Picquet et al., 1998; Ravishankara and Davis, 1978; Sørensen et al., 2002;

335 Wallington and Kurylo, 1987; Wayne and Tully, 1988; Wu et al., 2003). For the determination of the
336 bimolecular rate coefficient, both absolute and relative rate methods have been employed. Early
337 published data were in large disagreement between each other (Campbell et al., 1976; Greenhill and
338 Ogrady, 1986; Overend and Paraskevopoulos, 1978; Wallington and Kurylo, 1987; Wayne and Tully,
339 1988) with the problem to become even more intense between the temperature dependent kinetic
340 studies (Greenhill and Ogrady, 1986; Wallington and Kurylo, 1987; Wayne and Tully, 1988).
341 Nevertheless, the latest temperature dependent studies by Jimenez et al. (2003), Dillon et al. (2005)
342 and Orkin et al. (2011) are in excellent agreement. It is worth mentioning that, to the best of our
343 knowledge, all the temperature dependent studies have been carried out using absolute rate methods
344 and thus the present work is the first temperature dependent study using relative rate methods.
345 Literature data have been reviewed by both NASA/JPL and IUPAC kinetics panels (Atkinson et al.,
346 2006; Burkholder et al., 2015). In particular, IUPAC panel has adopted two different expression
347 depending on the temperature region of interest: $k(210 - 300 \text{ K}) = 3.2 \times 10^{-12} \exp(\frac{20}{T})$
348 $\text{cm}^3/(\text{molecule}\cdot\text{sec})$ and $k(216 - 599 \text{ K}) = 6.7 \times 10^{-18} T^2 \exp(\frac{511}{T}) \text{cm}^3/(\text{molecule}\cdot\text{sec})$ (Atkinson
349 et al., 2006). On the other hand, NASA/JPL panel preferred values are based on the comprehensive
350 absolute rate coefficient measurements at sub-ambient temperatures by Jiménez et al. (2003), Dillon et
351 al. (2005) and Orkin et al (2011). Therefore, a temperature independent reaction rate coefficient
352 ($k(210 - 298 \text{ K}) = 3.35 \times 10^{-12} \text{ cm}^3/(\text{molecule}\cdot\text{sec})$ (Burkholder et al., 2015)) is recommended
353 between 210 and 298 K.

354 In the current study, the kinetics of OH reaction with ethanol were studied in THALAMOS within the
355 temperature range of 263 to 353 K, using OH + *n*-pentane as reference reaction. The SIFT-MS was
356 employed for the real time monitoring of ethanol and the reference compound using the mass peaks 45
357 ($\text{C}_2\text{H}_5\text{O}^+$) and 42 (C_3H_6^+) employing NO^+ and O_2^+ precursor ions chemistry, respectively (see also
358 **Table 1**). The temperature dependent rate coefficients for the reference reaction have been adopted
359 from the recent review study from Morin et al. (2015) and was $k_{(\text{OH}+n\text{-pentane})} = 9.0 \times 10^{-17} \times$
360 $T^{1.8} \exp(\frac{120}{T}) \text{ cm}^3/(\text{molecule}\cdot\text{sec})$. The initial concentrations of ethanol and reference compound were

361 between 3 – 4.5 ppmV, while H₂O₂ was ranged between 90-500 ppmV. The summary of the
362 experimental conditions and the rate coefficients values obtained are given in **Table 2**. Typical relative
363 rate kinetic profiles are shown in **Fig. 3**, the NO⁺ and O₂⁺ precursor ions were selected to monitor the
364 concentrations of ethanol and pentane respectively. The lines are linear least-squares fits of the data
365 and the fit results are given in **Table 2**. The rate coefficient values determined in the current study,
366 along with the recommended literature values from IUPAC and NASA/JPL are depicted in **Fig. 4**. One
367 can notice an excellent agreement between the measured rate coefficients and the IUPAC and
368 NASA/JPL recommended values ($\pm 3\%$) within the entire temperature range experiments performed.
369 Therefore, it is evidenced that THAMALOS is capable of determining the rate coefficient of OH
370 initiated reactions as a function of temperature.

371 2.1.2 Cl atoms reaction rate coefficients with DCM.

372 The rate coefficient for the reaction of Cl atoms with DCM has been widely studied and kinetic data
373 are very well-established (Beichert et al., 1995; Bryukov et al., 2003; Catoire et al., 1996; Clyne and
374 Walker, 1973; Davis et al., 1970; Niki et al., 1980; Orlando, 1999; Sarzyński et al., 2011; Tschuikow-
375 Roux et al., 1988). Both absolute and relative rate measurements have been carried out to determine
376 the temperature dependent rate coefficient (see **Fig. 5**). The reported data have been reviewed by
377 IUPAC and NASA/JPL kinetics evaluation panels and the recommended expressions are k (220 –
378 300 K) = $5.9 \times 10^{-12} \exp(-\frac{850}{T})$ cm³/(molecule·sec) (IUPAC) and k (273 – 790 K) = $7.4 \times$
379 $10^{-12} \exp(-\frac{910}{T})$ cm³/(molecule·sec) (NASA/JPL).

380 In the current study, the rate coefficient for the gas phase reaction of Cl atoms with DCM was
381 measured as a function of temperature using two reference compounds, i.e., methane (CH₄) ($k_{(\text{methane} +$
382 $\text{Cl})} = 7.1 \times 10^{-12} \exp(-1270/T)$ cm³/(molecule·sec), NASA/JPL recommended over 181-1550 K)
383 and acetone (CH₃C(O)CH₃) ($k_{(\text{acetone} + \text{Cl})} = 1.63 \times 10^{-11} \exp(-\frac{610}{T})$ cm³/(molecule·sec),
384 recommended by NASA/JPL panel (Burkholder et al., 2015)). Furthermore, a series of experiments
385 were carried out at room temperature using 2,2,2-trifluoroethanol (CF₃CH₂OH) as reference, an
386 average value of $k_{(\text{trifluoroethanol} + \text{Cl})} = 6.85 \pm 0.8 \times 10^{-13}$ cm³/(molecule·sec) was calculated from
387 literature studies at 298 K (Garzón et al., 2010; Papadimitriou et al., 2003; Sellevåg et al., 2004) to

388 cross validate the rate coefficients measured using SIFT-MS and FTIR as detection techniques. The
389 SIFT-MS mass peaks used to monitor the reactants are summarized **Table 1**. FTIR kinetics analysis
390 was carried out employing the subtraction method in which the recorded spectra during reactions
391 progress were subtracted from scaled to the initial compounds concentration reference spectra
392 recorded, separately, for each compound. In all the cases, multiple bands for DCM and $\text{CH}_3\text{C}(\text{O})\text{CH}_3$
393 or $\text{CF}_3\text{CH}_2\text{OH}$ were monitored and it was ensured that the selected peaks were zeroed. Products
394 contribution was either subtracted, where possible, or taken into account in cases where interference
395 was intense and hard to resolve. Experiments at which differential IR spectroscopy was employed
396 were also carried out. In that case products appeared as positive peaks, while reactants as negative.
397 Differential analysis also led to indiscernible results. The experimental conditions and the rate
398 coefficient values determined are given in **Table 2**. Typical relative rate profiles are presented in
399 Appendix A **Fig. S3** and rate coefficients are summarized in the Arrhenius plot (**Fig. 5**). Kinetic
400 results from the present study are in excellent agreement with the corresponding recommended
401 literature data from both IUPAC and NASA/JPL kinetics evaluation panels within 4%.

402 To conclude, in this section has been evidenced that THALAMOS is capable of measuring accurate
403 gas phase rate coefficients of atmospheric relevant reactions as a function of temperature. To the best
404 of our knowledge, on European level there is no other simulation chamber that has been used for gas
405 phase kinetic studies in such a wide temperature range. Therefore, THALAMOS appears to be an
406 innovative reference tool for temperature dependent investigation of atmospheric relevant processes
407 extending and completing the capabilities of ASCs. Finally, we also present the kinetic and
408 mechanistic investigation of Cl atoms initiated reaction with toluene, as a function of temperature.

409 2.2 Cl atoms reaction rate coefficients with toluene

410 In this section, temperature dependent Cl kinetics and reaction products with toluene, a common
411 anthropogenic pollutant, are presented. Besides kinetics, product yields of benzaldehyde and benzyl
412 alcohol - primary oxidation products - as a function of temperature were also determined, and a
413 detailed mechanistic scheme is proposed.

414 2.2.1 Rate coefficient measurements

415 To the best of our knowledge, there are only room temperature kinetics studies for the reaction of Cl
416 atoms with toluene in the literature (Atkinson and Aschmann, 1985; Fantechi et al., 1998; Markert and
417 Pagsberg, 1993; Noziere et al., 1994; Shi and Bernhard, 1997; Wallington et al., 1988). In this work,
418 the rate coefficients of the Cl reaction with toluene were determined between 253 and 333 K, at 1 atm
419 (zero air) employing relative rate methods. Cl reaction with ethane, methanol, and butanone were used
420 as references, and their temperature dependent rate coefficients were taken from IUPAC kinetic
421 database (Atkinson et al., 2006), i.e., $k_{(\text{ethane} + \text{Cl})} = 7.05 \times 10^{-11} \exp(-\frac{60}{T}) \text{ cm}^3/(\text{molecule}\cdot\text{sec})$
422 recommended over 180-330 K; $k_{(\text{methanol} + \text{Cl})} = 7.10 \times 10^{-11} \exp(-\frac{75}{T}) \text{ cm}^3/(\text{molecule}\cdot\text{sec})$
423 recommended over 200-500 K; $k_{(\text{butanone} + \text{Cl})} = 3.05 \times 10^{-11} \exp(\frac{80}{T}) \text{ cm}^3/(\text{molecule}\cdot\text{sec})$ recommended
424 over 200-450 K, where $k_{(\text{M} + \text{Cl})}$ is the rate coefficient of the Cl reaction with the compound M.
425 Reactants loss and stable products formation were monitored via SIFT-MS. In particular, toluene,
426 methanol and butanone, were monitored using all the three precursor ions of the MS, i.e. H_3O^+ , NO^+
427 and O_2^+ , and the characteristic mass intensities of each compound are given in **Table 1**. Consequently,
428 the relative rate ratios were determined for each pair of precursor ions for toluene ($k_{\text{toluene}}^{\text{precursor ion}}$) and
429 the reference compound ($k_{\text{reference}}^{\text{precursor ion}}$) i.e., $k_{\text{toluene}}^{\text{H}_3\text{O}^+}/k_{\text{reference}}^{\text{H}_3\text{O}^+}$, $k_{\text{toluene}}^{\text{NO}^+}/k_{\text{reference}}^{\text{NO}^+}$ and $k_{\text{toluene}}^{\text{O}_2^+}/$
430 $k_{\text{reference}}^{\text{O}_2^+}$, respectively. The reported relative rate ratio represents the averaged value of the ions'
431 precursor ratio. However, in the cases that ethane was used as reference ($k_{\text{ethane}}^{\text{precursor ion}}$) and due to the
432 low proton transfer affinity of the H_3O^+ and NO^+ (low detection sensitivity), only O_2^+ precursor ion
433 was selected to monitor its concentration. Therefore, the relative rate ratios are given by the
434 expressions $k_{\text{toluene}}^{\text{H}_3\text{O}^+}/k_{\text{ethane}}^{\text{O}_2^+}$, $k_{\text{toluene}}^{\text{NO}^+}/k_{\text{ethane}}^{\text{O}_2^+}$ and $k_{\text{toluene}}^{\text{O}_2^+}/k_{\text{ethane}}^{\text{O}_2^+}$, while the mean relative rate
435 coefficients were obtained by averaging the values of the aforementioned fractions. **Table 3**
436 summarizes the conditions that experiments carried out, the relative rate ratios and the obtained rate
437 coefficients at each temperature. Typical relative rate kinetic profiles at 293 K are presented in **Fig. 6**.
438 The lines are linear least-squares fits of the data and the fit results are given in **Table 3**. It should be
439 pinpointed that as shown in **Fig. 6** a slight deviation from straight line fitting was observed, when

440 butanone was used as reference compound. This trend is a model-example that demonstrates
441 vulnerability of RR methods when compounds or references might be involved in secondary processes
442 (e.g photolysis, on-surface or gas phase hydrolysis, polymerization etc.). Therefore, although the
443 measurements, in which butanone was used as reference, lead to reasonable kinetic results, within the
444 measurements uncertainties, the number of the experiments were limited.

445 The results from this study are comparatively given in **Fig. 7**, along with the existing literature data. It
446 is evident that our room temperature values are in excellent agreement with the ones in the literature.
447 Averaged rate coefficient at 295 ± 3 K was measured to be $(5.82 \pm 0.19) \times 10^{-11}$ cm³/(molecule·sec). In
448 addition, no temperature dependence of the reaction rate coefficient was measured for the reaction of
449 Cl atoms with toluene between 253 and 333 K, leading to a value $(5.85 \pm 0.12) \times 10^{-11}$
450 cm³/(molecule·sec). The latter suggests a complex reaction mechanism that proceeds via adduct
451 formation. Although no temperature dependent experimental data exist in the literature Huang et al.
452 (2012) have theoretically studied the reaction using ab-initio calculations reporting a strong positive
453 temperature dependence of the rate coefficient in the range 298 – 1000 K. However, there are no data
454 available at lower temperatures. The authors propose that the reaction mainly proceeds through -H
455 atom abstraction from the methyl group of toluene (Huang et al., 2012).

456 2.2.2 Product Study and proposed reaction mechanism

457 The mechanistic investigation and product analysis of the Cl atoms reaction with toluene was carried
458 out in the temperature range 273 – 333 K using SIFT-MS as detection technique. Benzaldehyde and
459 benzyl alcohol were identified as primary degradation products. Traces of benzyl hydroperoxide were
460 also observed. The precursor ions and the mass spectral intensities used for the products detection with
461 the MS are given in **Table 1**. All products were quantified using MS that was calibrated by (i) flowing
462 a standard reference gas mixture, e. g., known concentration for each compound (toluene,
463 benzaldehyde and benzyl alcohol) or (ii) by injecting known amount of the compounds (in the liquid
464 or gas phase as mixture diluted in air as discussed in section admission and mixing of compounds)
465 inside THALAMOS and following their concentration with SIFT-MS. The second calibration method
466 was applied in order to account for the impact of temperature on the calibration factor of the

467 compounds. It should be noted that at sub-ambient temperatures, benzyl alcohol was not calibrated,
468 since it was very lossy on the wall surfaces due to the low vapor pressure (<0.2 Torr at 293 K and ca.
469 1.6 Torr at 333 K). Therefore, the calibration factor determined at room temperature was used to
470 estimate the corresponding product-yields. The estimated error to the concentration measurements was
471 ~7% for toluene and benzaldehyde, and ~15% for benzyl alcohol due to its sticky nature. Benzyl
472 hydroperoxide was not available and the MS calibration was not feasible. Therefore, the theoretical
473 concentrations included in the instrument's software were used instead. In addition, separate
474 photolysis tests for benzaldehyde and benzyl alcohol in the chamber were carried out leading to
475 negligible photolysis rates ($k_{\text{phot}} \sim 10^{-5} \text{ sec}^{-1}$) in the temperature range 273 – 333 K.

476 Typical temporal profiles for toluene consumption and benzaldehyde and benzyl alcohol formation are
477 presented in Appendix A **Fig. S4**, at 333 K. It is worth to note that although benzaldehyde was rapidly
478 produced, benzyl alcohol was appeared to be formed at delayed times when substantial toluene
479 consumption took place. This delayed production of Benzyl alcohol suggests either that benzyl alcohol
480 is a secondary reaction product or/and, less importantly, delayed mixing due to its low volatility. In
481 order to further look into benzyl alcohol formation, separate measurements carried out, in which the
482 reaction mixture was irradiated for ~ 10 min and then lights were off until benzyl alcohol reach a
483 steady state. The above cycle was repeated several times, until toluene consumption due to its reaction
484 with Cl atoms to be at least 50%.

485 Furthermore, to complement and cross validate the results obtained with the MS, an experiment was
486 carried out at room temperature coupling the FTIR to the chamber. The concentrations of toluene and
487 molecular chlorine used were rather high, in the range of 55 ppmV each. Benzaldehyde and benzyl
488 alcohol were also identified by FTIR. HCl was also observed to be formed. The reference spectra of
489 toluene and the formed organics were recorded in separate experiments after introducing a known
490 concentration of each compound in the FTIR cell. Toluene and benzaldehyde concentrations were
491 determined using the well-established cross section values at 739.8 and 1731 cm^{-1} for toluene and
492 benzaldehyde, respectively. Although benzyl alcohol was observed FTIR detection sensitivity was not
493 adequate to accurately measure its concentration. Toluene total loss was approximately 45%. Typical

494 IR spectra recorded during the reaction, as well as reference spectra of toluene, benzaldehyde and
495 benzyl alcohol are given in Appendix A **Fig. S5**.

496 **Table 4** summarizes the experimental conditions and the yields of the major products in the
497 temperature range 273 – 333 K. The yield of the detected products (Y_{DP}) was determined as the ratio of
498 the product concentration formed to the concentration of toluene consumed during the course of the
499 reaction:

$$500 \quad Y_{DP} = \Delta[\text{product}]/\Delta[\text{toluene}] \quad (3)$$

501 where $\Delta[\text{product}]$ correspond to the concentration of the product formed and $\Delta[\text{toluene}]$ the consumed
502 concentration of toluene.

503 It should be noted that product yields determination was based on the initial data of the photo-
504 oxidation experiment, where Cl atoms are principally consumed by toluene and side reactions of the
505 products formed with Cl atoms are negligible compared to formation rate, within the experimental
506 uncertainties. Benzaldehyde was found to be the major product formed. Typical plots displaying the
507 consumption of toluene and the formation of benzaldehyde with the SIFT-MS and the FTIR are given
508 in **Fig. 8**. The total yield of benzaldehyde was independent of temperature with an average value of
509 0.80 ± 0.05 (**Fig. 8**). The yield of benzyl alcohol was measured to be ~ 0.11 at 293 K (Appendix A **Fig.**
510 **S6**). At 273 K the yield of benzyl alcohol was decreased by a factor of 2 compared to the room
511 temperature value, but this might be an artifact of the system due to the high sticky efficiency and the
512 significantly decreased vapor pressure of the compound at lower temperatures. Regarding benzyl
513 hydroperoxide, an upper limit of 0.001 can be given based on the theoretical concentrations measured
514 with SIFT-MS.

515 There is a large disagreement between literature studies regarding the absolute yield of the products
516 formed from the Cl initiated oxidation of toluene. Nozière et al. (1994) conducted experiments in a
517 140 L Pyrex reactor using relatively high concentrations of toluene (6-33 ppmV) and Cl_2 (132 ppmV),
518 and they observed benzaldehyde, as the major product, with a yield of 0.41 ± 0.04 . The formation of
519 benzyl alcohol, and benzyl hydroperoxide was also reported with yields 0.15 ± 0.03 and 0.18 ± 0.04 ,

520 respectively (Noziere et al., 1994). On the contrary, Fantechi et al. (1998) did not detect either benzyl
521 alcohol or benzyl hydroperoxide. According to these authors, the major end-oxidation product was
522 benzaldehyde with a yield of 0.62 ± 0.30 . Wang et al. (2005), recently, reported product-yields for
523 benzaldehyde and benzyl alcohol of 0.84 ± 0.07 and 0.11 ± 0.02 , respectively. The benzyl
524 hydroperoxide formation was not included in Wang et al.'s analysis (Wang et al., 2005). However,
525 under their experimental conditions (i.e. atmospheric pressure and 296 K) benzyl hydroperoxide
526 concentration is expected to be very low, especially since the total products yield is almost unity (0.95
527 ± 0.08). The product yields measured in the current study at 293 K for benzaldehyde and benzyl
528 alcohol are in excellent agreement with those of Wang et al. (2005). In addition, no temperature
529 dependence of the yields was observed. although the upper limit for benzyl hydroperoxide (0.001) is
530 significantly lower than the reported value by Nozière et al. (1994), it is in agreement with the
531 observations from Fantechi et al. (1998) and Wang et al. (2005). Although Wang et al. (2005)
532 suggested that dark reactions in Nozière et al.'s system (1994) might be responsible for the observed
533 discrepancy, there are no evidence and the issue is currently unresolved (due to high initial
534 concentrations of toluene and Cl_2 used) .

535 Taking into account that the major products formed from the Cl initiated oxidation of toluene
536 preserved the aromatic structure and that no chlorinated organic compounds were observed, it seems
537 that reaction proceeds via direct or indirect -H atom abstraction and not by addition of Cl to the
538 aromatic ring. The formation of HCl observed in our FTIR experiment, as well as in other studies
539 (Fantechi et al., 1998) provide with further indications that enhance the latter statement's validity.
540 Further, a comparison between benzene ($k = 1.3 \times 10^{-15} \text{ cm}^3/(\text{molecule}\cdot\text{sec})$ at 295 K (Shi and
541 Bernhard, 1997) or $< 5.0 \times 10^{-16}$ (Noziere et al., 1994)) and toluene determined in this work ($k = 5.82$
542 $\times 10^{-11} \text{ cm}^3/(\text{molecule}\cdot\text{sec})$ at 298 K) was conducted, and reactivity towards Cl atoms reveals that
543 association mechanism is a highly unlikely reaction pathway and the replacement of one hydrogen
544 with a methyl group drastically increases toluene's reactivity, since - CH_3 hydrogen metathesis does
545 not affect ring's aromaticity. However, it is worth to mention that in order to further investigate if the
546 hydrogen metathesis proceeds via adduct formation in a stepwise process or via direct abstraction

547 quantomechanical molecular calculations could be of use, although it was beyond the scope of the
548 present study. Theoretical calculations performed by Huang et al. (2012) also support the experimental
549 observations. In particular, it is proposed that the -H atom is mainly abstracted from the -CH₃ group of
550 toluene, while the rest of the potent -H atom elimination sites, such as ortho, meta and para positions
551 have a negligible contribution if any. The latter is also consistent with previously reported
552 experimental studies (Fantechi et al., 1998; Markert and Pagsberg, 1993; Wang et al., 2005). Thus in
553 **Fig. 9**, a mechanistic scheme is proposed for the oxidation of toluene from Cl atoms.

554 Assuming that toluene is mainly removed from the atmosphere via the gas phase reactions with OH
555 radicals and Cl atoms, and reactions with O₃ and NO₃ are expected to be negligible, the atmospheric
556 lifetime (τ_x , where x is the corresponding oxidant) can be estimated using the expressions:

$$557 \quad \tau_{\text{OH}} = \frac{1}{k_{\text{OH}} \times [\text{OH}]} \quad (4)$$

558 and

$$559 \quad \tau_{\text{Cl}} = \frac{1}{k_{\text{Cl}} \times [\text{Cl}]} \quad (5)$$

560 where k_{OH} and k_{Cl} are the bimolecular rate coefficients for the corresponding reactions of toluene
561 with OH radicals (i.e. 6.12×10^{-12} cm³/(molecule·sec) at 300 K) and Cl atoms (i.e. 5.82×10^{-11}
562 cm³/(molecule·sec) at 295 ± 3 K average value of all studies) and [OH] and [Cl] are the diurnally
563 averaged concentrations of OH radicals and Cl atoms in the environment of reference. Assuming an
564 average tropospheric concentration of OH, i.e. 2×10^6 radical/cm³ and an average boundary layer
565 concentration of Cl, i.e. 10^4 atom/cm³ respectively, (Hein et al., 1997), OH radicals are expected to be
566 the dominant sink, leading to an estimated lifetime of about one day (1 day). In urban and coastal
567 areas though, where Cl atoms abundance is significant higher (Spicer et al., 1998), Cl chemistry will
568 substantially reduce the globally averaged lifetime of toluene, even locally, in the troposphere (**Table**
569 **5**), which might be important for such short-lived compounds. On the contrary, in indoor
570 environments where OH radical concentrations are significant lower, e.g., 10^4 to 10^5 molecule/cm³

571 (Carslaw, 2007; Sarwar et al., 2002) and Cl levels substantially increased due to the use of Cl-
572 containing cleaning products and other indoor materials, Cl atoms might dominate over OH radicals.

573

574 3. Conclusions

575

576 In the current study, we present a recently designed and developed photochemical chamber,
577 THALAMOS, with a wide temperature range thermostatic ability, 233 – 373 K. THALAMOS is
578 equipped with in-line FTIR, SIFT-MS and GC-MS complementary detection techniques that allow
579 internal cross-validation of various type of quantitative measurements, such as kinetics and product
580 yields studies. A detailed description of the facility, the instrumentation and the characterization of the
581 conditions has been realized. The first kinetic results employing relative rate methods obtained during
582 THALAMOS validation are also presented. Applying the relative rate method, and studying the
583 temperature dependence of two well documented reactions it was evident that THALAMOS is capable
584 of producing highly precise and accurate temperature kinetic data for atmospheric relevant OH and Cl
585 reactions. Furthermore, the kinetics and the mechanism for the Cl reaction with toluene was studied
586 within a wide temperature range. The kinetic measurements carried out in THALAMOS revealed that
587 the degradation of toluene from Cl atoms is important in coastal areas and/or indoor environments.
588 Benzaldehyde and benzyl alcohol were identified as the major Cl initiated end-oxidation products and
589 the yields were measured to be 0.80 ± 0.05 and 0.11 ± 0.04 , respectively. The present results are in
590 excellent agreement with the ones from Wang et al.⁴³ THALAMOS is oriented to be a unique tool for
591 temperature dependent studies in the gas or heterogeneous phases, targeted to elucidate the impact of
592 temperature to secondary organic aerosol formation, as well as to simulate extreme temperatures and
593 humidity conditions (i.e. $T > 25^{\circ}\text{C}$, $\text{RH} > 60\%$, typical for Southern countries). The latter aims to test
594 the efficiency of depolluting materials and to assist in sensors calibrations under extreme indoor or
595 outdoor conditions.

596

597 Acknowledgments

598 This article is dedicated to the memory of Dr. Ian Barnes from the Institute for Atmospheric
599 and Environmental Research, University of Wuppertal, Germany, one among the leaders of chemical
600 kinetics who inspired many scientists of our generation. This work is part of the chemical and physical
601 properties of the atmosphere (CaPPA) project funded by the Agence Nationale de la Recherche (ANR)
602 through the programme d'investissements d'avenir PIA (No. ANR-11-LABX-0005-01), the “Hauts-de-
603 France” Regional Council and the European Regional Development Fund (ERDF). A. Tomas and M.
604 Romanias are thankful to the Institut National des Sciences de L'univers (INSU) les Enveloppes
605 Fluides et L'environnement- Chimie de L'atmosphère (LEFE-CHAT) program for financial support. N.
606 Osseiran acknowledges support from Labex CaPPA for his graduate fellowship. V.C Papadimitriou
607 acknowledges support from Labex CaPPA for his short term visit at the institute mines telecom (IMT)
608 Lille Douai. M. E. Angelaki acknowledges support from the project make our planet great again
609 (MOPGA) for her short term visit at IMT Lille Douai, and the Greek sate scholarships foundation
610 (IKY) program that funds her PhD.

611

612

References

- Akimoto, H., Hoshino, M., Inoue, G., Sakamaki, F., Washida, N., Okuda, M., 1979. Design and characterization of the evacuable and bakable photochemical smog chamber. *Environ. Sci. Technol.* 13, 471-475.
- Atkinson, R., Aschmann, S.M., 1985. Kinetics of the gas phase reaction of Cl atoms with a series of organics at 296 ± 2 K and atmospheric pressure. *Int. J. Chem. Kinet.* 17, 33-41.
- Atkinson, R., Baulch, D.L., Cox, R.A., Crowley, J.N., Hampson, R.F., Hynes, R.G., et al., 2006. Evaluated kinetic and photochemical data for atmospheric chemistry: Volume II - gas phase reactions of organic species. *Atmos. Chem. Phys.* 6, 3625-4055.
- Beichert, P., Wingen, L., Lee, J., Vogt, R., Ezell, M.J., Ragains, M., et al., 1995. Rate constants for the reactions of chlorine atoms with some simple alkanes at 298 K: Measurement of a self-consistent set using both absolute and relative rate methods. *J. Phys. Chem.* 99, 13156-13162.
- Bryukov, M.G., Slagle, I.R., Knyazev, V.D., 2003. Kinetics of reactions of Cl atoms with ethane, chloroethane, and 1,1-dichloroethane. *J. Phys. Chem. A* 107, 6565-6573.
- Burkholder, J. B., Sander, S. P., Abbatt, J., Barker, J.R., Huie, R.E., Kolb, C.E., et al., 2015. Chemical kinetics and photochemical data for use in atmospheric studies, Evaluation No. 18, in: JPL Publication 15-10, Jet Propulsion Laboratory (Ed.), Pasadena.
- Campbell, I.M., McLaughlin, D.F., Handy, B.J., 1976. Rate constants for reactions of hydroxyl radicals with alcohol vapours at 292 K. *Chem. Phys. Lett.* 38, 362-364.
- Can, E., Özden Ü.Ö., Döğeroğlu, T., Gaga, E.O., 2015. Indoor air quality assessment in painting and printmaking department of a fine arts faculty building. *Atmos. Pollut. Res.* 6, 1035-1045.
- Carslaw, N., 2007. A new detailed chemical model for indoor air pollution. *Atmos. Environ.* 41, 1164-1179.
- Catoire, V., Lesclaux, R., Schneider, W. F., Wallington, T. J., 1996. Kinetics and mechanisms of the self-reactions of CCl_3O_2 and CHCl_2O_2 radicals and their reactions with HO_2 . *J. Phys. Chem.* 100, 14356-14371.
- Clyne, M.A.A., Walker, R.F., 1973. Absolute rate constants for elementary reactions in the chlorination of CH_4 , CD_4 , CH_3Cl , CH_2Cl_2 , CHCl_3 , CDCl_3 and CBrCl_3 . *J. Chem. Soc., Faraday Trans.* 1 69, 1547-1567.
- Davis, D.D., Braun, W., Bass, A.M., 1970. Reactions of $\text{Cl}_2\text{P}^{3/2}$: Absolute rate constants for reaction with H_2 , CH_4 , C_2H_6 , CH_2Cl_2 , C_2Cl_4 , and $c\text{-C}_6\text{H}_{12}$. *Int. J. Chem. Kinet.* 2, 101-114.
- Dillon, T.J., Hölscher, D., Sivakumaran, V., Horowitz, A., Crowley, J.N., 2005. Kinetics of the reactions of HO with methanol (210–351 K) and with ethanol (216–368 K). *Phys. Chem. Chem. Phys.* 7, 349-355.
- Fantechi, G., Jensen, N.R., Saastad, O., Hjorth, J., Peeters, J., 1998. Reactions of Cl atoms with selected VOCs: Kinetics, products and mechanisms. *J. Atmos. Chem.* 31, 247-267.
- Garzón, A., Moral, M., Notario, A., Ceacero-Vega, A.A., Fernández-Gómez, M., Albaladejo, J., 2010. Atmospheric reactions of (H)- and (D)-fluoroalcohols with chlorine atoms. *Chem. Phys. Chem.* 11, 442-451.
- Greenhill, P.G., Ogrady, B.V., 1986. The rate-constant of the reaction of hydroxyl radicals with methanol, ethanol and (D_3)methanol. *Aust. J. Chem.* 39, 1775-1787.
- Hazrati, S., Rostami, R., Fazlzadeh, M., Pourfarzi, F., 2016. Benzene, toluene, ethylbenzene and xylene concentrations in atmospheric ambient air of gasoline and CNG refueling stations. *Air Qual. Atmos. Health* 9, 403-409.
- Hein, R., Crutzen, P. J., Heimann, M., 1997. An inverse modeling approach to investigate the global atmospheric methane cycle. *Global Biogeochem. Cycles* 11, 43-76.
- Huang, M., Wang, Z., Hao, L., Zhang, W., 2012. DFT study on the abstraction and addition of Cl atom with toluene. *Comput. Theor. Chem.* 996, 44-50.
- Jiménez, E., Gilles, M.K., Ravishankara, A.R., 2003. Kinetics of the reactions of the hydroxyl radical with CH_3OH and $\text{C}_2\text{H}_5\text{OH}$ between 235 and 360 K. *J. Photochem. Photobiol. A* 157, 237-245.
- King, M., 2016. The relative-rate technique for determining rate constants. ECG Environ. Briefs ECGEB No 13.

Kovács, G., Szász-Vadász, T., Papadimitriou, V. C., Dóbbé, S., Bérces, T., Márta, F., 2005. Absolute rate constants for the reactions of OH radicals with $\text{CH}_3\text{CH}_2\text{OH}$, $\text{CF}_2\text{HCH}_2\text{OH}$ and $\text{CF}_3\text{CH}_2\text{OH}$. *React. Kinet. Catal. Lett.* 87, 129-138.

Leone, J.A., Flagan, R.C., Grosjean, D., Seinfeld, J.H., 1985. An outdoor smog chamber and modeling study of toluene- NO_x photooxidation. *Int. J. Chem. Kinet.* 17, 177-216.

Lide, R. D. , 2005. *Physical Constants of Organic Compounds*, in: *CRC Handbook of Chemistry and Physics* (85th Ed.). CRC Press.

Markert, F., Pagsberg, P., 1993. UV spectra and kinetics of radicals produced in the gas phase reactions of Cl, F and OH with toluene. *Chem. Phys. Lett.* 209, 445-454.

Morin, J., Romanias, M.N., Bedjanian, Y., 2015. Experimental study of the reactions of OH radicals with propane, n-pentane, and n-heptane over a wide temperature range. *Int. J. Chem. Kinet.* 47, 629-637.

United Nations, 2018. *World urbanization prospects 2018: The speed of urbanization around the world*.

Nelson, L., Rattigan, O., Neavyn, R., Sidebottom, H., Treacy, J., Nielsen, O.J., 1990. Absolute and relative rate constants for the reactions of hydroxyl radicals and chlorine atoms with a series of aliphatic alcohols and ethers at 298 K. *Int. J. Chem. Kinet.* 22, 1111-1126.

Niki, H., Maker, P.D., Savage, C.M., Breitenbach, L.P., 1980. An FTIR study of the Cl atom-initiated oxidation of CH_2Cl_2 and CH_3Cl . *Int. J. Chem. Kinet.* 12, 1001-1012.

Noziere, B., Lesclaux, R., Hurley, M.D., Dearth, M.A., Wallington, T.J., 1994. A kinetic and mechanistic study of the self-reaction and reaction with HO_2 of the benzylperoxy radical. *J. Phys. Chem.* 98, 2864-2873.

Oh, S., Andino, J.M., 2001. Kinetics of the gas-phase reactions of hydroxyl radicals with C1–C6 aliphatic alcohols in the presence of ammonium sulfate aerosols. *Int. J. Chem. Kinet.* 33, 422-430.

Orkin, V.L., Khamaganov, V.G., Martynova, L.E., Kurylo, M.J., 2011. High-accuracy measurements of OH• reaction rate constants and IR and UV absorption spectra: Ethanol and partially fluorinated ethyl alcohols. *J. Phys. Chem. A* 115, 8656-8668.

Orlando, J.J., 1999. Temperature dependence of the rate coefficients for the reaction of chlorine atoms with chloromethanes. *Int. J. Chem. Kinet.* 31, 515-524.

Overend, R., Paraskevopoulos, G., 1978. Rates of hydroxyl radical reactions. 4. Reactions with methanol, ethanol, 1-propanol, and 2-propanol at 296 K. *J. Phys. Chem.* 82, 1329-1333.

Papadimitriou, V.C., Prosmittis, A.V., Lazarou, Y.G., Papagiannakopoulos, P., 2003. Absolute reaction rates of chlorine atoms with $\text{CF}_3\text{CH}_2\text{OH}$, $\text{CHF}_2\text{CH}_2\text{OH}$, and $\text{CH}_2\text{FCH}_2\text{OH}$. *J. Phys. Chem. A* 107, 3733-3740.

Picquet, B., Heroux, S., Chebbi, A., Doussin, J.F., Durand-Jolibois, R., Monod, A., et al., 1998. Kinetics of the reactions of OH radicals with some oxygenated volatile organic compounds under simulated atmospheric conditions. *Int. J. Chem. Kinet.* 30, 839-847.

Ravishankara, A.R., Davis, D.D., 1978. Kinetic rate constants for the reaction of hydroxyl with methanol, ethanol, and tetrahydrofuran at 298 K. *J. Phys. Chem.* 82, 2852-2853.

Sarwar, G., Corsi, R., Kimura, Y., Allen, D., Weschler, C.J., 2002. Hydroxyl radicals in indoor environments. *Atmos. Environ.* 36, 3973-3988.

Sarzyński, D., Gola, A.A., Brudnik, K., Jodkowski, J.T., 2011. Kinetic study of the reaction of chlorine atoms with dichloromethane and D-dichloromethane in the gas phase. *Chem. Phys. Lett.* 514, 220-225.

Sellevåg, S.R., Nielsen, C.J., Søvde, O.A., Myhre, G., Sundet, J.K., Stordal, F., et al., 2004. Atmospheric gas-phase degradation and global warming potentials of 2-fluoroethanol, 2,2-difluoroethanol, and 2,2,2-trifluoroethanol. *Atmos. Environ.* 38, 6725-6735.

Shi, J., Bernhard, M. J., 1997. Kinetic studies of Cl-atom reactions with selected aromatic compounds using the photochemical reactor-FTIR spectroscopy technique. *Int. J. Chem. Kinet.* 29, 349-358.

Smith, D., Spanel, P., 2005. Selected ion flow tube mass spectrometry (SIFT-MS) for on-line trace gas analysis. *Mass Spectrom. Rev.* 24, 661-700.

Sørensen, M., Hurley, M.D., Wallington, T.J., Dibble, T.S., Nielsen, O.J., 2002. Do aerosols act as catalysts in the OH radical initiated atmospheric oxidation of volatile organic compounds? *Atmos. Environ.* 36, 5947-5952.

- Spanel, P., Smith, D., 2013. Advances in on-line absolute trace gas analysis by SIFT-MS. *Curr. Anal. Chem.* 9, 524.
- Tschuikow-Roux, E., Faraji, F., Paddison, S., Niedzielski, J., Miyokawa, K., 1988. Kinetics of photochlorination of mono- and disubstituted fluoro-, chloro-, and bromomethanes. *J. Phys. Chem.* 92, 1488-1495.
- Wallington, T.J., Kurylo, M.J., 1987. The gas phase reactions of hydroxyl radicals with a series of aliphatic alcohols over the temperature range 240–440 K. *Int. J. Chem. Kinet.* 19, 1015-1023.
- Wallington, T.J., Skewes, L.M., Siegl, W.O., 1988. Kinetics of the gas phase reaction of chlorine atoms with a series of alkenes, alkynes and aromatic species at 295 K. *J. Photochem. Photobiol. A* 45, 167-175.
- Wang, L., Arey, J., Atkinson, R., 2005. Reactions of chlorine atoms with a series of aromatic hydrocarbons. *Environ. Sci. Technol.* 39, 5302-5310.
- Wayne, P.H., Tully, F.P., 1988. Catalytic conversion of alcohols to alkenes by OH. *Chem. Phys. Lett.* 152, 183-189.
- Wu, H., Mu, Y., Zhang, X., Jiang, G., 2003. Relative rate constants for the reactions of hydroxyl radicals and chlorine atoms with a series of aliphatic alcohols. *Int. J. Chem. Kinet.* 35, 81-87.

Table 1 Mass spectral ions intensities selected to monitor the concentration profiles of the compounds used in the current study.

Compound	Product ions used monitored	Mass to charge ratio (m/z)	Precursor ion
Ethanol	$C_2H_5O^+$	45	NO^+
<i>n</i> -Pentane	$C_3H_6^+$	42	O_2^+
Dichloromethane (DCM)	$CH(^{35}Cl)(^{35}Cl)^+$	83	NO^+
Acetone	$C_3H_6O^+$	58	O_2^+
2,2,2-Trifluoroethanol	$[CF_3CH_2OH]H^+$	101	H_3O^+
Methane	$CH_3O_2^+$	47	O_2^+
Toluene	$C_7H_8H^+$	93	H_3O^+
	$C_7H_8^+$	92	NO^+
	$C_7H_8^+$	92	O_2^+
Ethane	$C_2H_4^+$	28	O_2^+
Methanol	CH_5O^+	33	H_3O^+
	NO^+CH_3OH	62	NO^+
	CH_3O^+	31	O_2^+
Butanone	$C_4H_9O^+$	73	H_3O^+
	$NO^+C_4H_8O$	102	NO^+
	$C_4H_8O^+$	72	O_2^+
Benzaldehyde	$C_7H_7O^+$	107	H_3O^+
	$C_7H_5O^+$	105	NO^+
	$C_7H_5O^+$	105	O_2^+
Benzyl alcohol	$C_7H_7^+$	91	H_3O^+
	$C_7H_8O^+$	108	NO^+
	$C_7H_8O^+$	108	O_2^+
Benzyl hydroperoxide	$C_7H_8O_2^+$	124	H_3O^+
	$NO^+C_7H_8O_2^+$	154	NO^+

Table 2 Experimental conditions and kinetics results for the gas phase reaction of OH radicals with ethanol and Cl atoms with DCM.

C₂H₅OH + OH					
<i>T</i> (K)	[Ethanol] ₀ (ppmV)	[Pentane] ₀ (ppmV)	[H ₂ O ₂] ₀ (ppmV)	<i>k</i> _{ethanol} / <i>k</i> _{pentane} ^a	<i>k</i> (×10 ⁻¹² cm ³ /(molecul e·sec)) ^b
263	3.1	3.0	300	1.04±0.01	3.35±0.03
278	3.2	3.0	90	0.97±0.01	3.37±0.03
293	3.5	3.4	250	0.93±0.01	3.40±0.04
	3.4	3.5	380	0.91±0.01	
	3.6	3.6	95	0.89±0.01	
313	3.7	3.7	90	0.85±0.01	3.48±0.04
333	4.0	3.9	450	0.81±0.01	3.63±0.04
353	4.2	4.1	500	0.77±0.01	3.75±0.05
CH₂Cl₂ + Cl					
Reference: methane. $k_{(\text{methane} + \text{Cl})} = 7.1 \times 10^{-12} \exp(-1270/T) \text{ cm}^3/(\text{molecule} \cdot \text{sec})$, JPL recommended over 181-1550 K					
<i>T</i> (K)	[DCM] ₀ (ppmV)	[Methane] ₀ (ppmV)	[Cl ₂] ₀ (ppmV)	<i>k</i> _{DCM} / <i>k</i> _{methane} ^a	<i>k</i> (×10 ⁻¹³ cm ³ /(molecul e·sec)) ^b
258	2.8	21	80	4.16±0.05	2.15±0.03
270	2.9	16.6	61	3.81±0.02	2.45±0.02
298	3.8	18.1	36	3.48±0.02	3.49±0.02
	3.2	20.8	40	3.50±0.02	
323	3.4	20	48	3.16±0.02	4.36±0.03
Reference: acetone. $k_{(\text{acetone} + \text{Cl})} = 1.63 \times 10^{-11} \exp(-610/T) \text{ cm}^3/(\text{molecule} \cdot \text{sec})$, JPL recommended over 210-440 K					
<i>T</i> (K)	[DCM] ₀ (ppmV)	[Acetone] ₀ (ppmV)	[Cl ₂] ₀ (ppmV)	<i>k</i> _{DCM} / <i>k</i> _{acetone} ^a	<i>k</i> (×10 ⁻¹³ cm ³ /(molecul e·sec)) ^b
253	2.7	1.0	56	0.15±0.01	2.22±0.14
273	2.9	1.0	34	0.16±0.01	2.72±0.17
298	3.2	1.1	6.3	0.18±0.01	3.79±0.21
298	1.9	0.6	7.4	0.17±0.01	3.57±0.21
323	3.4	1.2	8.0	0.19±0.01	4.68±0.24
353	2.28	0.7	17	0.19±0.01	6.08±0.28
Reference: 2,2,2-trifluoroethanol. $k_{(\text{trifluoroethanol} + \text{Cl})} = (6.85 \pm 0.8) \times 10^{-13} \text{ cm}^3/(\text{molecule} \cdot \text{sec})$ at 298 K					
<i>T</i> (K)	[DCM] ₀ (ppmV)	[Trifluoroethanol] ₀ (ppmV)	[Cl ₂] ₀ (ppmV)	<i>k</i> _{DCM} / <i>k</i> _{trifluoroethanol} ^a	<i>k</i> (10 ⁻¹³) ^b
298	2.1	1.1	6.0	0.52±0.01	3.56±0.07
298	1.1	0.7	5.0	0.51±0.01	3.49±0.07
298 (FTIR)	15	15	88	0.49±0.02	3.35±0.14

^a Errors represent the 2σ precision from the least-squares fits and do not include systematic uncertainties.

^bErrors reflects the 2σ precision of the relative rate ratio measurements and do not include any systematic uncertainty.

[M]₀: initial concentration of the compound M; *T*: temperature; *k*_{ethanol} / *k*_{pentane}: the experimentally determined relative rate coefficient ratios of the ethanol and the reference compound; *k*_{DCM} / *k*_{methane}, *k*_{DCM} / *k*_{acetone}, and *k*_{DCM} / *k*_{trifluoroethanol}: the experimentally determined relative rate coefficient ratios of

DCM and the three reference compounds used (i.e. methane, acetone, trifluoroethanol), respectively; $k_{(\text{methane} + \text{Cl})}$, $k_{(\text{acetone} + \text{Cl})}$, and $k_{(\text{trifluoroethanol} + \text{Cl})}$: the rate coefficients of methane, acetone and trifluoroethanol with Cl atoms as proposed in literature; k : is the final value of the rate coefficient of the compound of interest; NASA/JPL: National Aeronautics and Space Administration/Jet Propulsion Laboratory.

Table 3 Summary of the experimental conditions and rate coefficients obtained in this work for the gas phase reaction of toluene with Cl atoms.

Reference: Ethane. $k_{(\text{ethane} + \text{Cl})} = 7.05 \times 10^{-11} \exp(-60/T)$, IUPAC recommended over 180-330 K									
T (K)	[Toluene] ₀ (ppmV)	[Ethane] ₀ (ppmV)	[Cl ₂] ₀ (ppmV)	$k_{\text{toluene}}^{\text{H}_3\text{O}^+}/k_{\text{ethane}}^{\text{O}_2^+}$ ^a	$k_{\text{toluene}}^{\text{NO}^+}/k_{\text{ethane}}^{\text{O}_2^+}$ ^a	$k_{\text{toluene}}^{\text{O}_2^+}/k_{\text{ethane}}^{\text{O}_2^+}$ ^a	Variation ^b	$k_{\text{toluene}}/k_{\text{ethane}}$ of all ions ^c	k ($\times 10^{-11}$ cm ³ /(molecule·sec)) ^c
253	3.3	3.3	22	1.14±0.08	1.16±0.08	1.19±0.04	4%	1.16±0.03	6.45±0.17
273	3.6	3.6	20	1.00±0.01	1.00±0.01	0.98±0.01	2%	0.99±0.01	5.60±0.06
293	3.8	3.8	15	1.02±0.02	1.01±0.01	1.03±0.01	2%	1.02±0.01	5.86±0.06
293	5.6	5.6	15	1.03±0.02	1.01±0.01	1.02±0.01	2%	1.02±0.01	
313	4.1	4.1	11	0.98±0.02	1.00±0.02	1.02±0.01	4%	1.00±0.02	5.82±0.12
333	4.3	4.3	17	0.99±0.04	1.00±0.04	0.99±0.02	1%	1.00±0.01	5.89±0.06
Reference: Methanol. $k_{(\text{methanol} + \text{Cl})} = 7.10 \times 10^{-11} \exp(-75/T)$, IUPAC recommended over 200-500 K									
T (K)	[Toluene] ₀ (ppmV)	[Methanol] ₀ (ppmV)	[Cl ₂] ₀ (ppmV)	$k_{\text{toluene}}^{\text{H}_3\text{O}^+}/k_{\text{methanol}}^{\text{H}_3\text{O}^+}$ ^a	$k_{\text{toluene}}^{\text{NO}^+}/k_{\text{methanol}}^{\text{NO}^+}$ ^a	$k_{\text{toluene}}^{\text{O}_2^+}/k_{\text{methanol}}^{\text{O}_2^+}$ ^a	Variation	$k_{\text{toluene}}/k_{\text{methanol}}$ of all ions ^c	k ($\times 10^{-11}$ cm ³ /(molecule·sec)) ^c
253	3.4	3.4	33	1.02±0.01	0.97±0.01	1.08±0.02	10%	1.02±0.06	5.38±0.32
268	3.3	4.1	17	1.20±0.01	1.07±0.02	1.18±0.01	11%	1.15±0.07	6.17±0.38
278	1.7	1.8	10	1.11±0.01	0.97±0.02	1.12±0.01	13%	1.07±0.08	5.80±0.43
278	3.5	4.5	20	1.06±0.01	1.04±0.02	1.10±0.01	5%	1.07±0.03	
293	1.9	2.0	11	1.08±0.01	0.96±0.02	1.07±0.01	11%	1.04±0.07	5.72±0.38
333	2.1	2.2	12	0.99±0.01	0.95±0.02	1.05±0.01	10%	1.00±0.05	5.68±0.28
Reference: Butanone. $k_{(\text{butanone} + \text{Cl})} = 3.05 \times 10^{-11} \exp(80/T)$, IUPAC recommended over 200-450 K									
T (K)	[Toluene] ₀ (ppmV)	[Butanone] ₀ (ppmV)	[Cl ₂] ₀ (ppmV)	$k_{\text{toluene}}^{\text{H}_3\text{O}^+}/k_{\text{butanone}}^{\text{H}_3\text{O}^+}$ ^a	$k_{\text{toluene}}^{\text{NO}^+}/k_{\text{butanone}}^{\text{NO}^+}$ ^a	$k_{\text{toluene}}^{\text{O}_2^+}/k_{\text{butanone}}^{\text{O}_2^+}$ ^a	Variation	$k_{\text{toluene}}/k_{\text{butanone}}$ of all ions ^c	k ($\times 10^{-11}$ cm ³ /(molecule·sec)) ^c
293	1.9	1.8	11	1.58±0.10	1.45±0.06	1.46±0.08	8%	1.50±0.07	6.22±0.31
293	1.9	1.8	11	1.72±0.06	1.60±0.04	1.51±0.04	12%	1.61±0.10	
313	1.8	1.9	7.0	1.52±0.02	1.51±0.04	1.27±0.02	16%	1.43±0.14	5.63±0.55
Average k ($\pm 2\sigma$) over the temperature range 258-333 K									5.85±0.15^d

^a Errors represent the 2 σ fit precision and do not include systematic uncertainties^b Variation denotes the difference between the highest and the lowest relative rate ratios of the compound of interest and the reference, $k_{\text{toluene}}/k_{\text{reference}}$, values between the different precursor ions.^c Uncertainties quoted to the mean values are the 2 σ standard deviations.

^d Quoted uncertainty is the 2σ precision of the average value obtained from the linear fit of all measurements (see **Fig. 7**).

The relative rate ratios determined for each pair of precursor ions (H_3O^+ , NO^+ and O_2^+) for toluene ($k_{\text{toluene}}^{\text{precursor ion}}$) and the reference compound ($k_{\text{reference}}^{\text{precursor ion}}$) are given in the table as $k_{\text{toluene}}^{\text{H}_3\text{O}^+}/k_{\text{reference}}^{\text{H}_3\text{O}^+}$, $k_{\text{toluene}}^{\text{NO}^+}/k_{\text{reference}}^{\text{NO}^+}$, and $k_{\text{toluene}}^{\text{O}_2^+}/k_{\text{reference}}^{\text{O}_2^+}$. The reported relative rate ratio represents the averaged value of the ions' precursor ratio.

Table 4 Summary of experimental conditions and product yields for the gas phase reaction of toluene with Cl atoms.

T (K)	[Toluene] ₀ (ppmV)	[Cl ₂] ₀ (ppmV)	Benzaldehyde					Benzyl alcohol			
			Yield ^{H₃O⁺} (%) ^a	Yield ^{NO⁺} (%) ^a	Yield ^{O₂⁺} (%) ^a	Average yield of all ions (%)	Yield FTIR (%) ^a	Yield ^{H₃O⁺} (%) ^a	Yield ^{NO⁺} (%) ^a	Yield ^{O₂⁺} (%) ^a	Average yield of all ions (%) ^b
273	4.0	10.0	82±8	72±7	80±8	78±5	nd ^b	5±1	4±1	6±1	5±1
293	4.0	10.0	88±9	90±9	84±8	87±3	nd	9±2	9±2	10±2	10±2
293	4.0	7.0	78±8	73±7	83±8	78±5		11±2	11±2	13±3	12±3
293	12.0	22.0	72±7	70±7	75±8	72±3		nd	nd	nd	nd
293	52.0	55.0	85±8	82±8	92±9	86±5	75±7	17±3	17±3	12±2	16±3
333	3.0	11.0	85±8	74±7	86±8	82±7	nd	13±3	11±2	14±3	13±2
333	3.0	9.0	90±9	85±8	82±8	86±4		10±2	12±2	14±3	12±2
Total yield (independent on T)							80±5^b				11±4^b

^a Errors represent the 2σ fit precision and includes the uncertainty to concentrations determination

^b Uncertainties quoted to the mean values are the standard deviation.

nd: not determined; Yield^{H₃O⁺}, Yield^{NO⁺} and Yield^{O₂⁺}: the yield of the products formed deploying selective ion flow tube mass spectrometry (SIFT-MS) for each of the precursor ions H_3O^+ , NO^+ and O_2^+ ; Average yield of all ions: the average yield of each product formation using SIFT-MS; Yield FTIR: the yield of benzaldehyde demined deploying Fourier transformed infrared spectroscopy (FTIR).

Table 5 Toluene atmospheric lifetime include both OH and Cl initiated tropospheric oxidation.

Scenario 1			Scenario 2		
τ_{OH} (hours)	τ_{Cl} (hours)	τ_{eff} (hours)	τ_{OH} (hours)	τ_{Cl} (hours)	τ_{eff} (hours)
22.7	955	22.2	22.7	47.7	15.4

Two different scenarios with regard the globally averaged diurnal OH radicals and Cl atoms concentrations have been employed. OH levels remained stable in both cases $[\text{OH}] 2 \times 10^6$ radical/cm³, while the extremes of diurnally averaged Cl concentration levels were used to include both free troposphere (Scenario 1: $[\text{Cl}] 5 \times 10^3$ atom/cm³) and local characteristics of urban and/or coastal environment (Scenario 2: $[\text{Cl}] 1 \times 10^5$ atom/cm³).

τ_{OH} , and τ_{Cl} : toluene atmospheric lifetime due to its degradation by OH radicals and Cl atoms respectively; τ_{eff} : the effective lifetime of toluene .

Figures

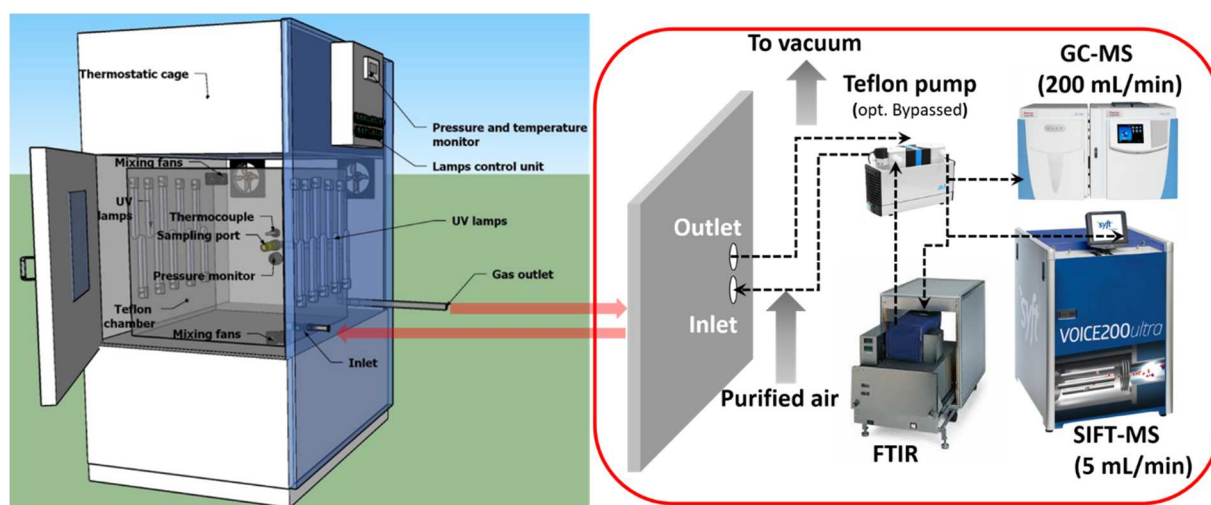


Fig. 1 General description of THALAMOS (thermally regulated atmospheric simulation chamber) facility. UV: ultraviolet; FTIR: Fourier transformed infrared spectroscopy; GC-MS: gas chromatography mass spectrometry; SIFT-MS: selective ion flow tube mass spectrometry.

Fig. 2.

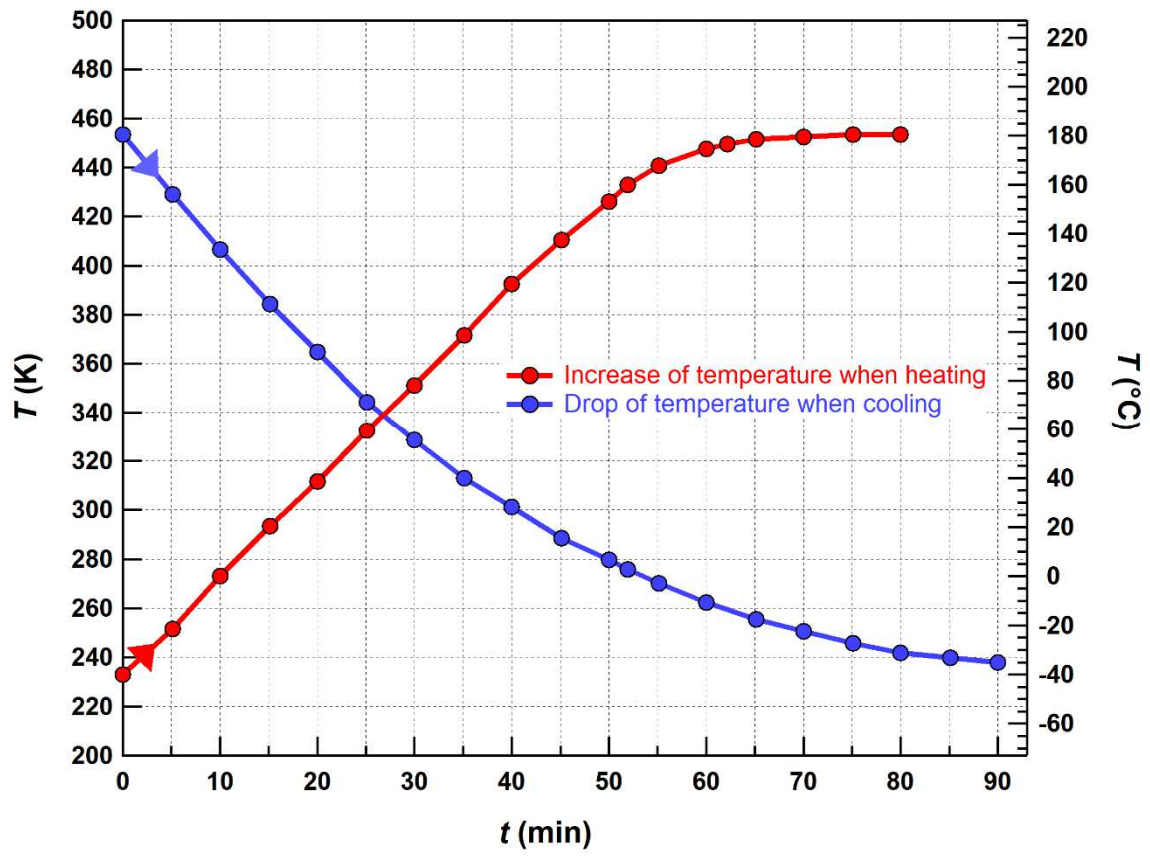


Fig. 2 Temperature (T) dynamic in the climatic box determined under heating and cooling experiments. The arrows placed at the beginning of each curve aim to display the corresponding process followed to determine the temperature change rate. t : time.

Fig. 3.

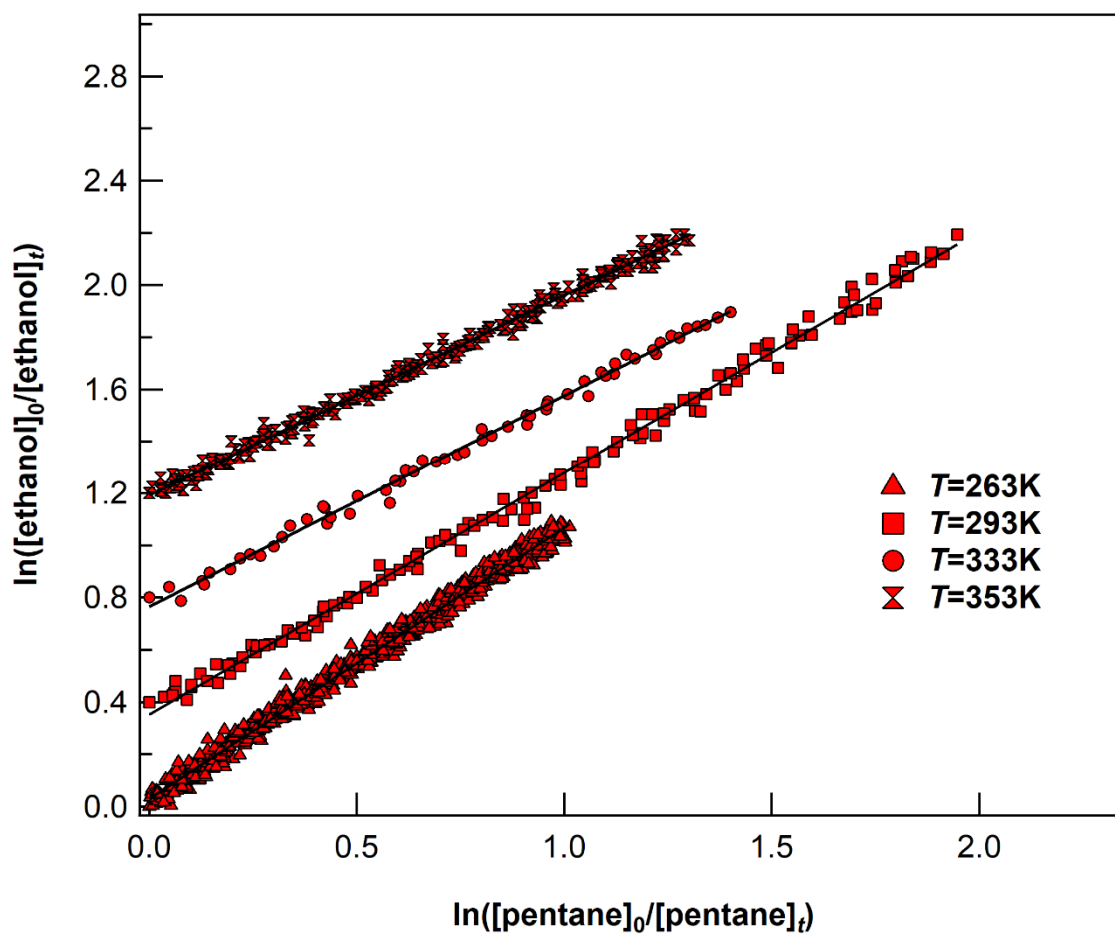


Fig. 3 Relative rate data for the reaction of OH + ethanol using pentane as reference molecule at 263, 293, 333 and 353 K respectively. For clarity, the experimental measurements are shifted up on the y axis by 0.4 for 293 K, 0.8 for 333 K and 1.2 for 353 K. $[\text{ethanol}]_0$, $[\text{pentane}]_0$, $[\text{ethanol}]_t$, $[\text{pentane}]_t$ are the initial concentrations of the compound of interest (ethanol) and that of the reference (pentane), with no OH radicals present (light-sources off), at $t = 0$ and at discrete reaction times t , respectively.

Fig. 4.

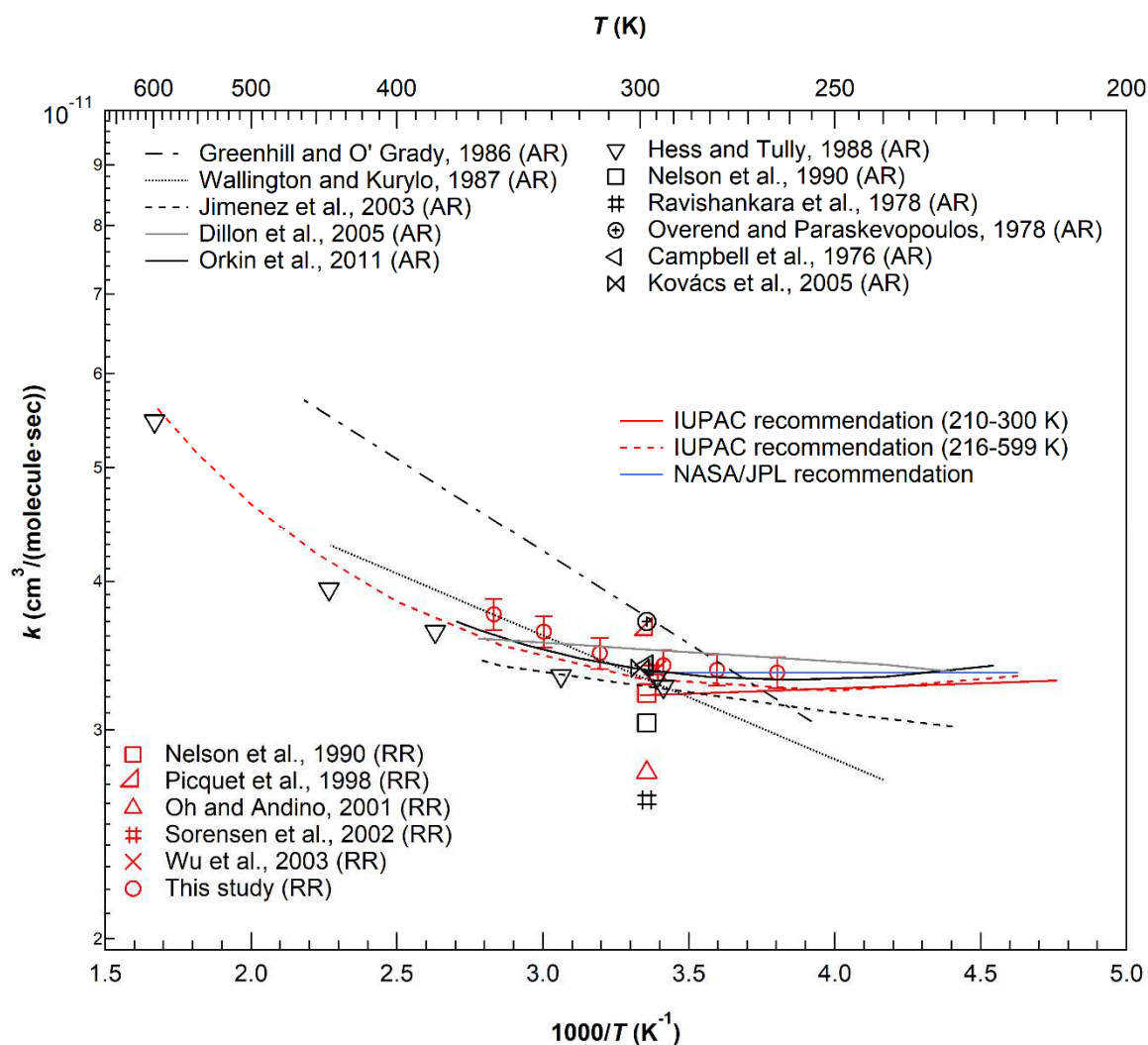


Fig. 4 Arrhenius plot for the OH + ethanol reaction. In comparison with the measurements of the current study, are displayed the literature results determined with absolute methods (AR) and relative rate methods (RR) as well as the International Union of Pure and Applied Chemistry (IUPAC) and the National Aeronautics and Space Administration/Jet Propulsion Laboratory (NASA/JPL) recommended values. For clarity purposes, the uncertainties on literature results are not given; only the 2σ precision of the measurements ($<2\%$) of the current study are displayed.

Fig. 5.

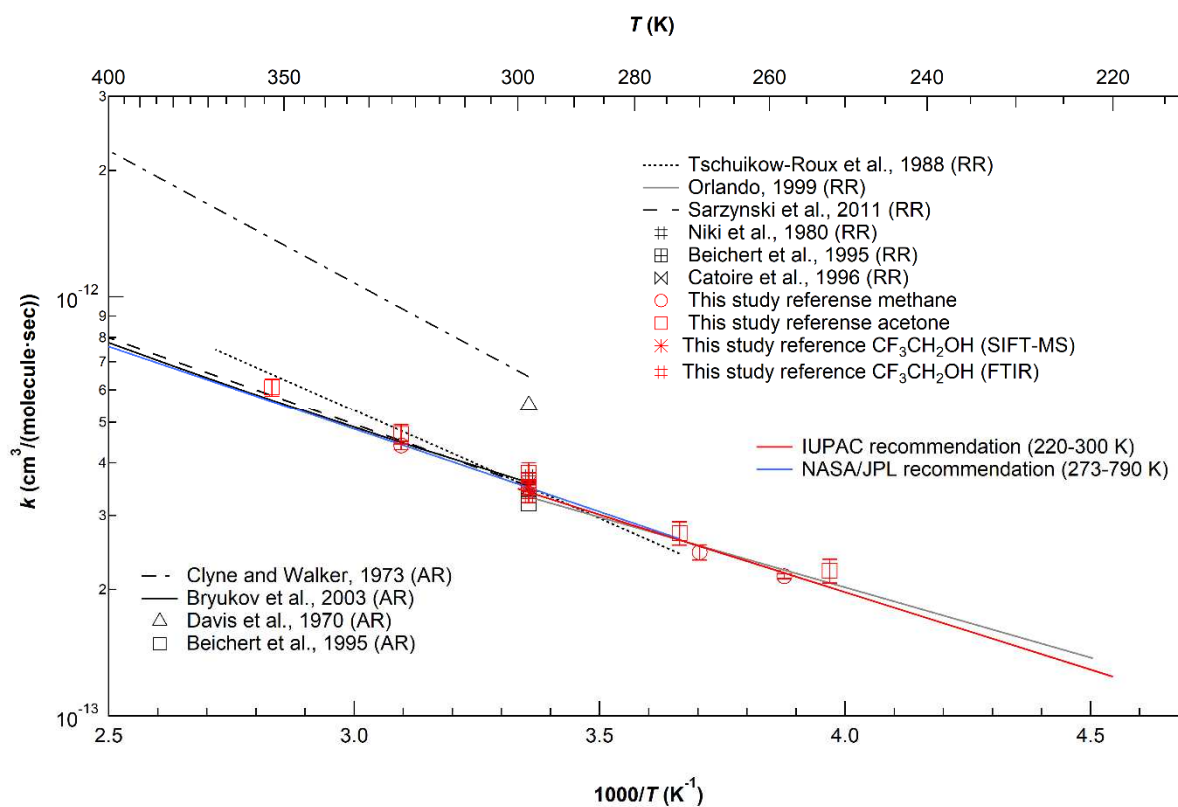


Fig. 5 Arrhenius plot for the reaction of Cl atoms with DCM. For clarity purposes the NASA/JPL recommended values above 400 K are not displayed.

Fig. 6.

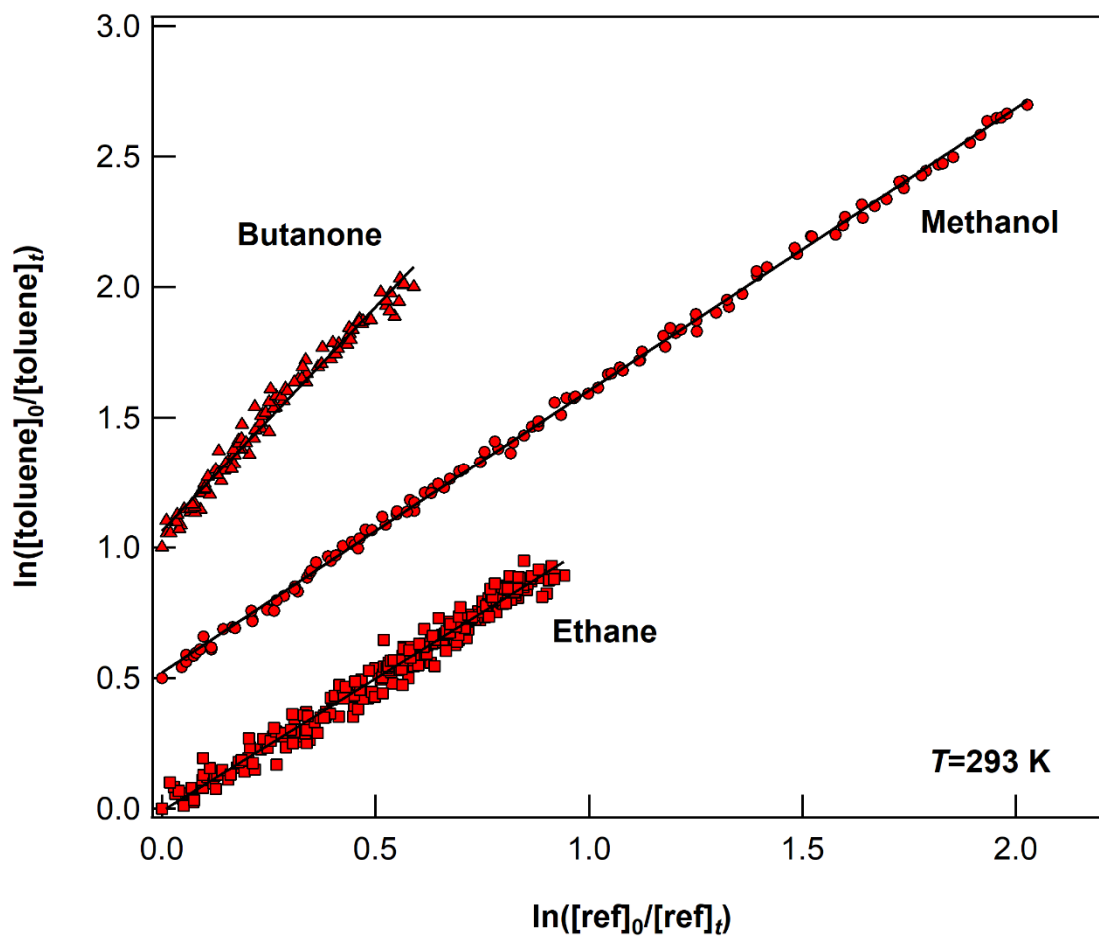


Fig. 6 Example of relative rate plots for the Cl + toluene reaction obtained at 293 K using the reference compounds labeled on the graph. For the relative rate data displayed, the H_3O^+ precursor ion of the SIFT-MS was selected to monitor in real time the concentrations of toluene and the reference. For clarity the measurements have been displaced vertically by 0.5 for methanol and 1 for butanone. $[\text{toluene}]_0$, $[\text{ref}]_0$, $[\text{toluene}]_t$, $[\text{ref}]_t$ are the initial concentrations of the compound of interest and that of the reference, with no OH radicals present (light-sources off), at $t = 0$ and at discrete reaction times t , respectively.

Fig. 7.

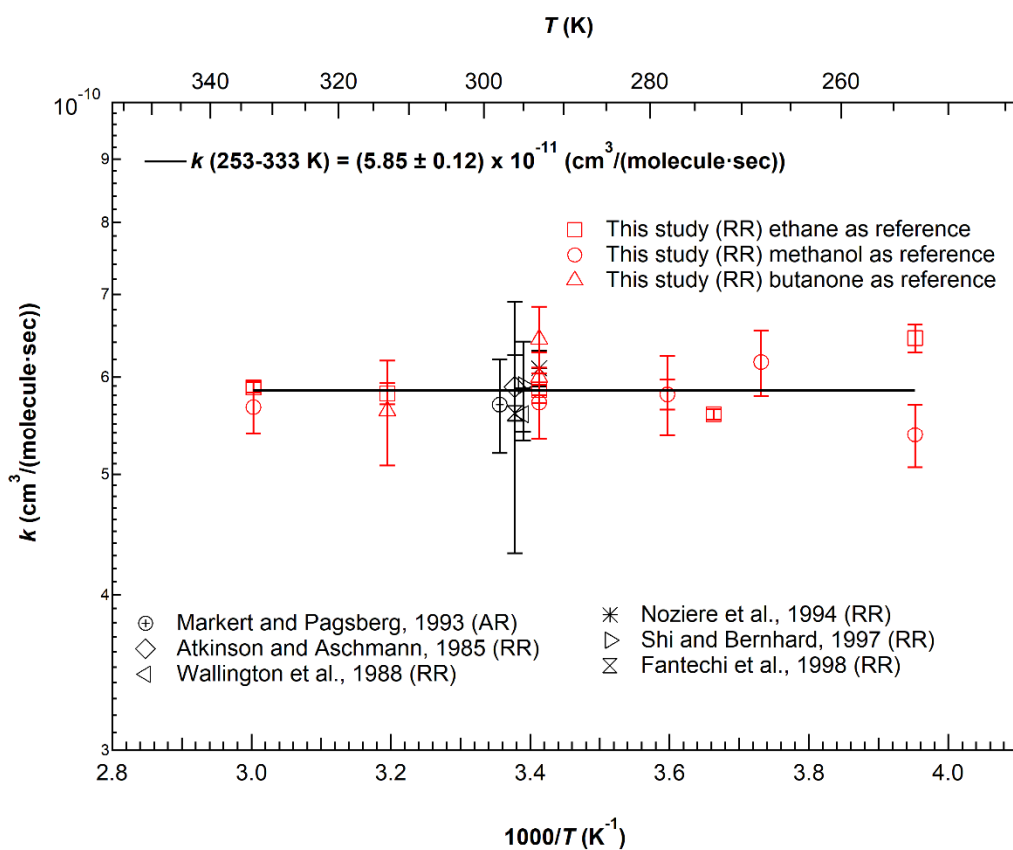


Fig. 7 Temperature dependent data for the reaction of Cl atoms with toluene. The error bars quoted in our measurements correspond to the standard deviation of the mean values determined for the different precursor ions. The solid line corresponds to the average value of all measurements performed in the range of 253 to 353 K.

Fig. 8.

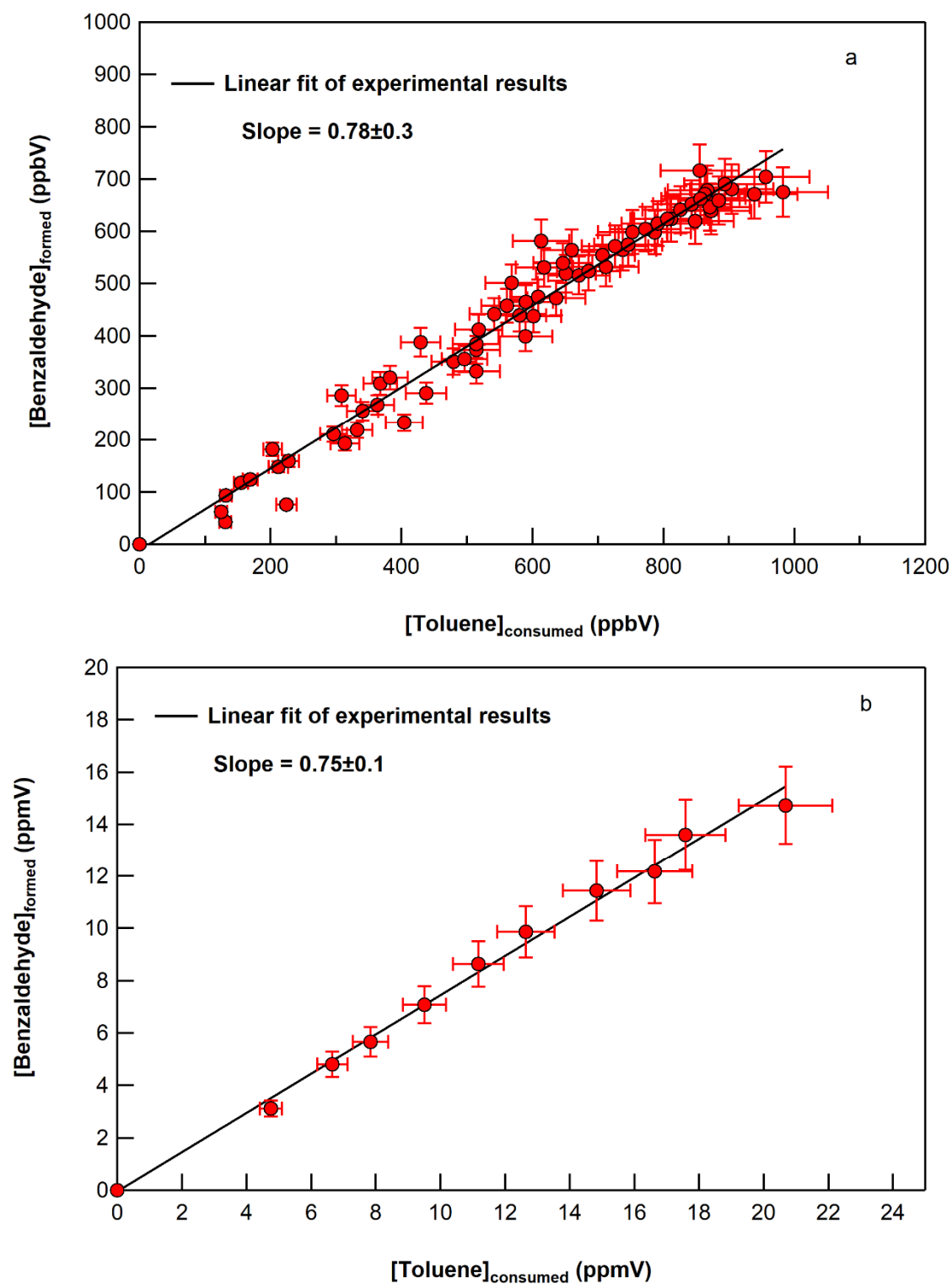


Fig. 8 Typical concentration plots of benzaldehyde formed versus toluene consumed at 293 K with (a) the SIFT-MS using the H_3O^+ precursor ion to monitor the corresponding compounds and (b) the FTIR. Error bars reflect the uncertainty to the determination of compounds concentrations. The lines are the

linear fit of experimental results (not forced to pass through the origin). The slope corresponds to the product yield of benzaldehyde ($\pm 2\sigma$ precision).

Fig. 9

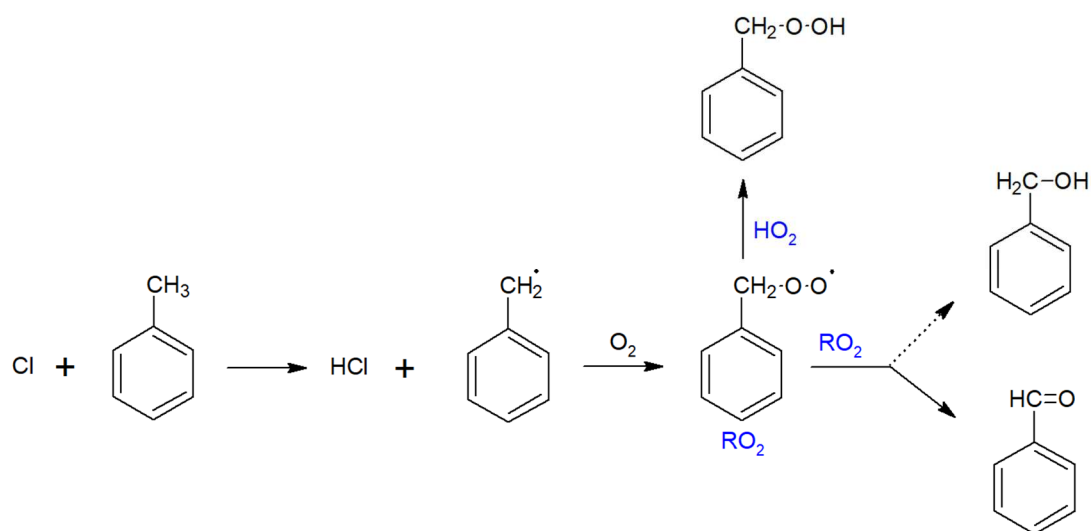


Fig. 9 Proposed reaction mechanism for the oxidation of toluene from Cl atoms. The dash arrow is used to indicate the possible formation of a secondary product.